2017-01-01

Improving The Regression Rate Of An Htpb Hybrid Rocket Fuel Grain

Travis Wesley Belcher
University of Texas at El Paso, travisb117@gmail.com

IMPROVING THE REGRESSION RATE OF AN HTPB HYBRID ROCKET FUEL GRAIN

TRAVIS BELCHER

Master's Program in Mechanical Engineering

APPROVED:

Norman Love, Ph.D., Chair

Ahsan R. Choudhuri, Ph.D.

Tzu-Liang Tseng, Ph.D.

Charles H. Ambler, Ph.D.
Dean of the Graduate School

Dedication

I would like to dedicate this work to the friends, family, colleagues, and teachers who have believed in me and stuck with me through this long journey.

IMPROVING THE REGRESSION RATE OF AN HTPB HYBRID ROCKET FUEL GRAIN

by

TRAVIS WESLEY BELCHER, B.S. Mechanical Engineering

THESIS

Presented to the Faculty of the Graduate School of

The University of Texas at El Paso

in Partial Fulfillment

of the Requirements

for the Degree of

MASTER OF SCIENCE

Department of Mechanical Engineering

THE UNIVERSITY OF TEXAS AT EL PASO

December 2017

Acknowledgements

I would like to thank the Missile Defense Agency for the financially supporting the project that generated this research. The material in this project is based upon the work supported by MDA under award HQ0147-15-C-6001 and any opinions, findings, conclusions, or recommendations expressed herein are those of the authors and do not necessarily reflect the views of the agency. I would also like to thank my advisors Dr. Norman Love and Dr. Ahsan Choudhuri for the opportunity to learn from them during my time here at UTEP. Further, I would like to thank my teammates, past and present, for the huge contributions they made to this effort, Jason Adams, Daniela Aguilar, Lucero Buendia, Raul Cervantes, Alan Esparza, Robert Ferguson, Edward Kang, Dylan Ott, Shyamal Patel, Norma Perea, Itzel Torres, Jonathan Valenzuela, Justin Vanhoose, and Alejandro Vazquez. A special thanks goes to my parents, friends, and family for their constant support and encouragement of me through my years of education.

Table of Contents

Acknowledgements v

List of Figures ix

List of Tables x

Chapter 1: Introduction 1

1.1 Liquid Bi-Propellant Systems 2

1.2 Solid Propellant Systems 5

1.3 Hybrid Rocket Systems 7

1.4 Hydroxyl Ammonium Nitrate 10

1.5 AF-M315E Green Monopropellant 11

1.6 Project Relevance 13

1.7 Project Objectives 14

Chapter 2: Background and Theory 15

2.1 Regression Rate 15

2.2 Regression Rate Improvement 20

2.3 HAN Decomposition 26

2.4 AF-M315E 30

Chapter 3: Experimental Methodology 31

3.1 Experimental Setup 31

3.1.1 Low Flow Test Setup 31
3.1.2 High Flow System Design 33
3.1.3 Delivery System 34
3.1.4 Steam Generating System 36
3.1.5 Methane Igniter 39
3.2 Test Article 42
3.2.1 Gas Mixing Chamber 42
3.2.2 Grain Adapter 47
3.3 GOX/HTPB Test Matrix 49
3.4 HAN Decomposition Products/HTPB Test Approach 51
3.5 Test Operations 52
Chapter 4: Chapter 4: Results and Analysis 55
4.1 Alterations to Testing Scope 55
4.2 Proof of Concept Test Results 57
4.3 Capability Study Test Results 58
4.4 Regression Rate 61
Chapter 5: Conclusion 64
5.1 Summary 64
5.2 Future Work 65
References 68

Appendix A: HAN CEA Code 71

Appendix B: Test Procedure 74

Appendix C: HTPB Motor Creation Procedure 84

Curriculum Vita 93

List of Figures

Figure 1.1: Simple Liquid Bi-Propellant System Diagram [4] 2
Figure 1.2: Galileo's “Simplified” Hypergolic Bi-Propellant System Schematic [4] 3
Figure 1.3: Solid Rocket Configuration with Each component labeled [4] 6
Figure 1.4: Typical Hybrid Rocket Configuration 8
Figure 2.1: Depiction of the boundary layer that forms inside of hybrid fuel grains [11] 16
Figure 2.2: Demonstration of the fuel grain being liquified, then vaporized in a hybrid rocket motor [11] 17
Figure 2.3: Regions of regression rate dependency [16] 19
Figure 2.4: Conceptual pintle injector design that is placed inside of the fuel grain and used to inject oxidizer 21
Figure 2.5: Conceptual co-axial swirl injector design that is placed inside of the fuel grain and used to inject oxidizer 22
Figure 2.6: Conceptual swirl injector design that is placed inside of the fuel grain and used to inject oxidizer 23
Figure 2.7: Thermal decomposition of 40% HAN solution [17] 27
Figure 2.8: Catalytic decomposition of 40% HAN solution [17] 27
Figure 2.9: Integrated photoion signals as a function of temperature for m/z 30 (nitric oxide) and m/z 33 (hyaluronic acid) on (a) copper 8.5-10.5 eV (b) copper 11.5-14.5 eV (c) iridium 8.5-10.5 eV (d) iridium 11.5-14.5 eV 28
Figure 3.1: Schematic diagram of the low flow system [10] 32
Figure 3.2: Picture of the low flow system 33
Figure 3.3: Delivery System Schematic 35
Figure 3.4: Exit Temperature of Steam from the Steam Generator as a function of Tube Length 38
Figure 3.5: Steam Generator System Schematic 39
Figure 3.6: UTEP's Patented CH4/GOX Ignitors 40
Figure 3.7: Engineer Diagram of UTEP's Patented CH4/GOX Ignitor [21] 41
Figure 3.8: Block Diagram of the Test Article 42
Figure 3.9: Inline Port Gas Mixing Chamber 43
Figure 3.10: Tangential Gas Mixing Chamber 44
Figure 3.11: Swirl Gas Mixing Chamber 45
Figure 3.12: Gas Swirl Mixing Chamber Cross-Section View 46
Figure 3.13: Fabricated Tangential Gas Mixing Chamber 47
Figure 3.14: Exploded View of the High Flow Grain Adapter 49
Figure 3.15: Three different phases of ignition (1) Ignitor ignition (2) Diffusion flame ignition (3) Self-sustained hybrid combustion 53
Figure 4.1: A Comparison of the Proof of Concept Testing to Previous Testing Data and Literature [10,29] 57
Figure 4.2: Graphical Results of Capability Testing 60
Figure 4.3: Compilation of Images During Testing 61
Figure 4.4: Regression Rate from Previous Experiments Compared to the Capability Test Series 62
Figure 5.1: Suggested Steam Generator Upgrade 66

List of Tables

Table 1.1: Experimental Data comparing various hybrid propellant combinations 10
Table 1.2: A comparison of several GPIM propellants to hydrazine 11
Table 2.1: Comparison of different hybrid Fuel/Oxidizer combinations [24] 24
Table 2.2: Results of the analysis of HAN decomposition using NASA's CEA code 28
Table 3.1: Proof of Concept Test Series Matrix 50
Table 3.2: Simulated HAN Decomposition Gases/HTPB Test Matrix 51
Table 3.3: Hybrid Rocket Automatic Test Sequence 52
Table 4.1: Proof of Concept Test Results 57
Table 4.2: Gas Mixture Testing Results 58
Table 4.3: Steam Mixture Testing Results 59
Table 4.4: Regression Rate Data for Capability Testing 62

Chapter 1: Introduction

Since the Chinese Sung Dynasty first began using rockets as weapons against the Mongolian Empire in the 13th century [1], the science of rocketry has grown to the point that human beings are on the verge of becoming a multi-planetary species. George Sutton defines Rocket Propulsion as, "a class of jet propulsion that produces thrust by ejecting stored matter, called the propellant [2]." The ambiguity of this definition allows for a very broad mixture of propellants in different states of matter to be utilized, depending on the mission profile of the rocket in question. There are a multitude of different styles of rocket engines currently being studied, from nuclear thermal rockets to monopropellants, but by and far, the most common types being used in industry are liquid bipropellant and solid rocket motors. With such a vast amount of industry experience surrounding these two rocket engine categories, it makes sense that experts would try to combine them to produce an amalgam of the two styles. This third style is simply referred to as a hybrid rocket engine, and quite a bit of research and development has been poured into it, despite the fact that its use has mostly been relegated to laboratory studies and amateur rocket enthusiasts. The focus of this thesis is on developing a hybrid rocket testing facility at the University of Texas at El Paso and innovating new ways of increasing the performance of hybrid rocket motors coupled with Green Propellant Oxidizers.

1.1 Liquid Bi-Propellant Systems

By and far, one of the more common propulsion systems, liquid systems, have a wide range of applications from large scale launch systems to in-space hypergol systems. The basic operation of a liquid system has a liquid or gaseous fuel and oxidizer being injected into a combustion chamber and ignited to release a large amount of pressure and heat, thus generating thrust. A premier example of a liquid bipropellant system is the Liquid Hydrogen/Liquid Oxygen (LOX) RS-25 engines used on NASA's Space Shuttle and upcoming Space Launch System (SLS) [3]. These systems have some of the highest specific impulses of all of the chemical propulsion systems, ranging from 290 to 450s. Additionally, their high propellant densities and the ability to throttle their thrust allows them to enjoy a wide range of mission profiles.

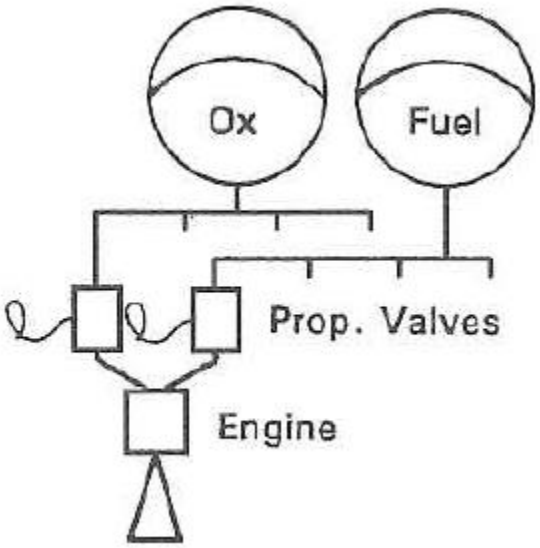

Figure 1.1: Simple Liquid Bi-Propellant System Diagram [4]

Despite their many advantages, liquid systems suffer from issues such as high complexity and high cost when compared to other chemical systems. The system complexity comes from the huge amount of plumbing required in order to properly direct the propellants, as

well as monitor and protect the system. The potential complexities of the system can be seen in Figure 1.2, with the simplified system schematic for Galileo's propulsion system.

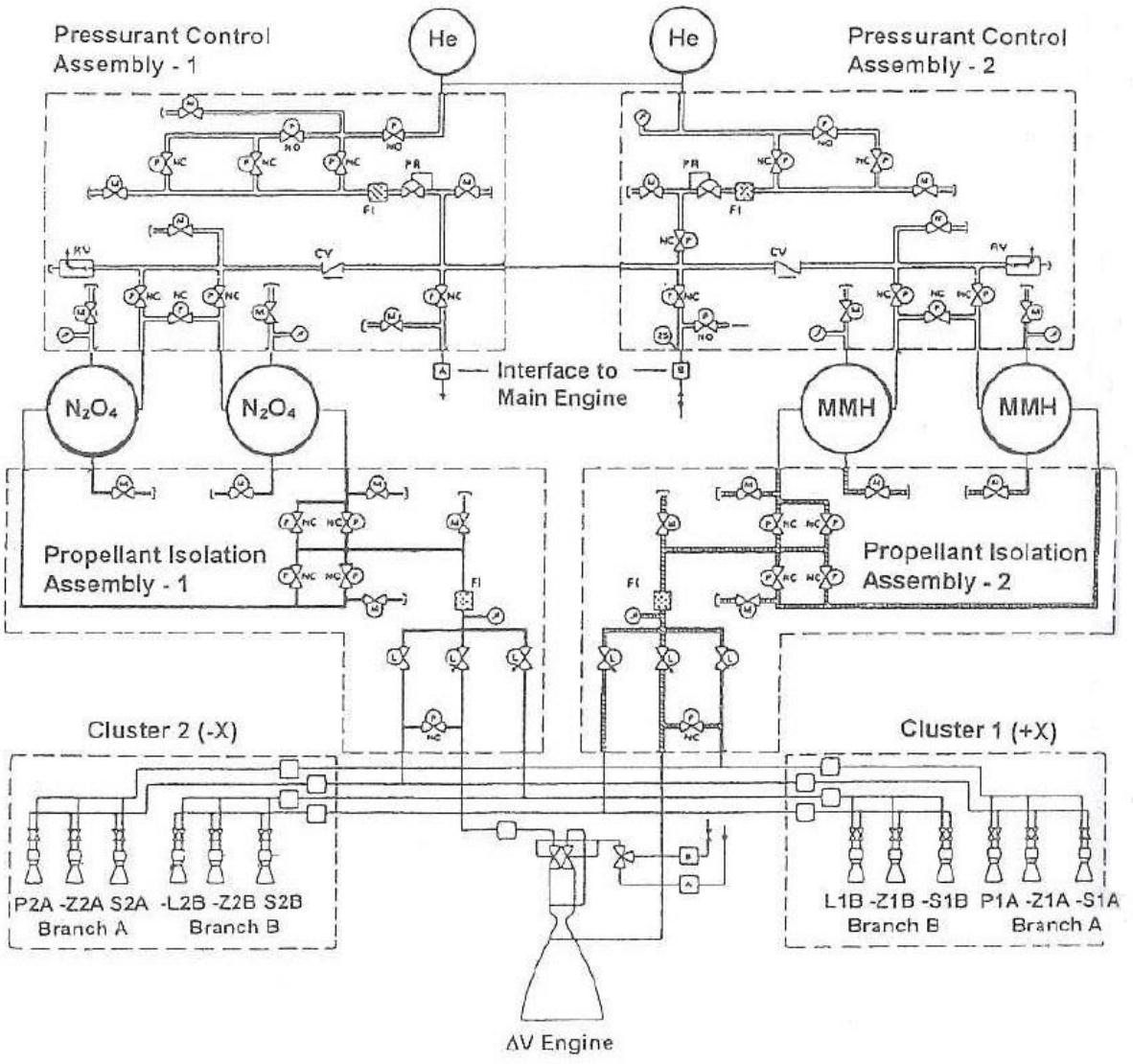

Figure 1.2: Galileo's "Simplified" Hypergolic Bi-Propellant System Schematic [4]

Additionally, to achieve the high performance desired of most launch systems, cryogenics are utilized to increase the propellant density, which further increases the system complexity and mass. All of this intricacy quickly drives up the cost to make them prohibitive in many applications.

Lastly, though liquid rocket engines are capable of throttling, the ranges through which they can throttle are generally narrow. Liquid engines are also notorious for suffering from combustion instabilities when operating at their ideal mixture ratio [8]. Throttling these engines exacerbates the problem and can cause extreme vibration and fatigue cycles on the vehicle or spacecraft they're propelling.

1.2 Solid Propellant Systems

Solid propellant systems also have a large presence in the chemical rocket community as they are used extensively as boosters to achieve atmospheric exit velocities, as well in space on satellites in order to drive them to higher orbits. These systems are extremely simple in that the fuel and oxidizer are mixed together and molded into a solid grain. The grain needs an ignition source in order to fire, once the reaction is initiated the grain will burn until it has completely exhausted the fuel source. This is both the bane and benefit of solid propellants, in that their weight is almost entirely propellant, which is entirely converted to thrust. However, the inability to halt the reaction of the fuel and oxidizer means that any rocket utilizing solid propellants is inherently hazardous.

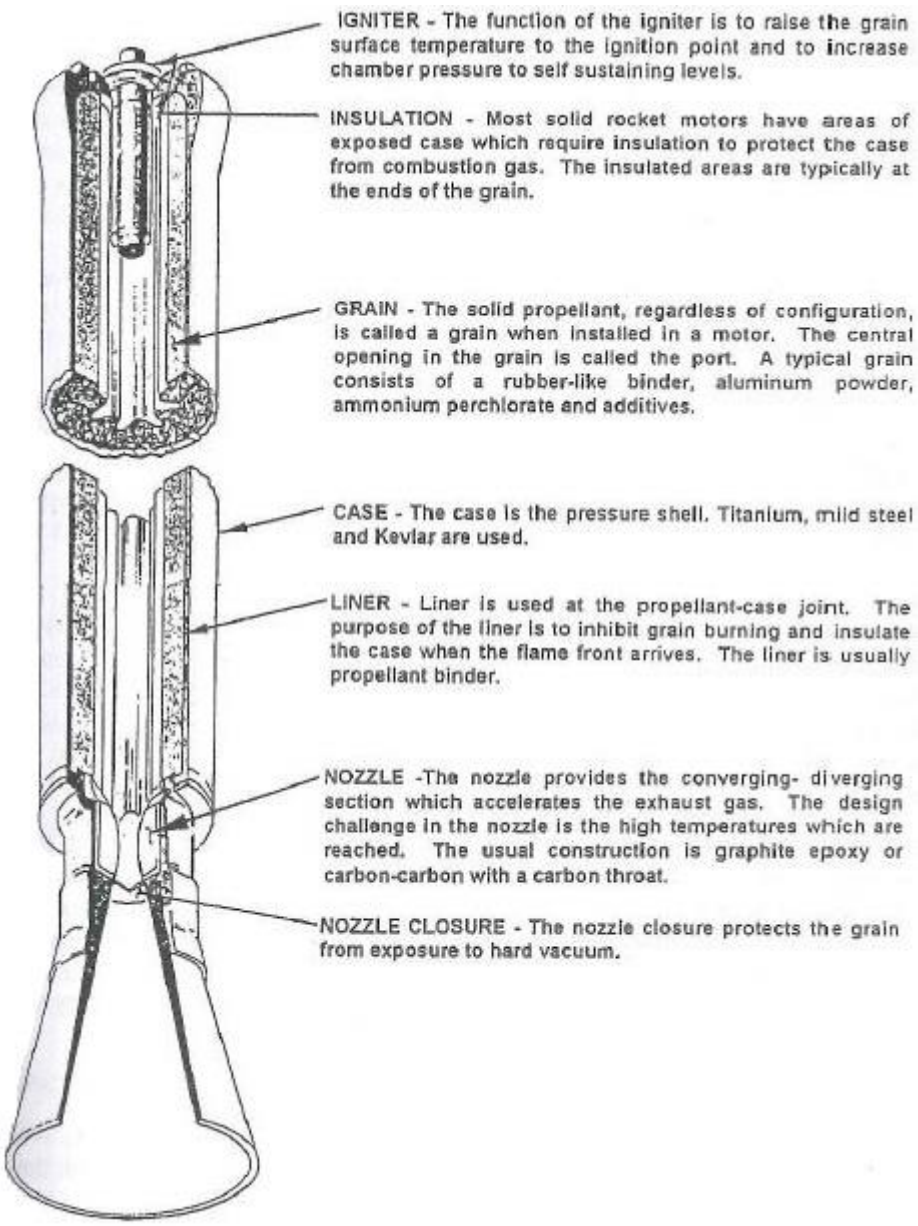

Figure 1.3: Solid Rocket Configuration with Each component labeled [4]

These inherent hazards require rigorous safety measures to be placed on storing and handling these motors to ensure that ignition is avoided. Furthermore, solid propellant systems lack the high specific impulses boasted by liquid bi-propellant systems due to their less energetic propellants.

1.3 Hybrid Rocket Systems

Hybrid rockets blend the characteristics of liquid and solid propellant systems, allowing them to reap some of the benefits of each system. A hybrid rocket is typically configured to have a solid fuel grain coupled with a liquid or gaseous oxidizer, similar to the system featured in Figure 1.4. The oxidizer flows over the fuel grain where the vaporized fuel particles leave the surface of the grain and are burned in the oxidizer flow stream, releasing heat and pressure to generate thrust. An ignitor is used to initiate the vaporization of the fuel grain which is then able to achieve a self-sustaining burn until it depletes all of its fuel, or the oxidizer flow is ceased. A variety of different types of ignitors are used to achieve this self-sustained burn. Commonly used ignitors are liquid/liquid torches, solid propellant squibs, or a hypergolic ignitor, such as TEA/TEB.

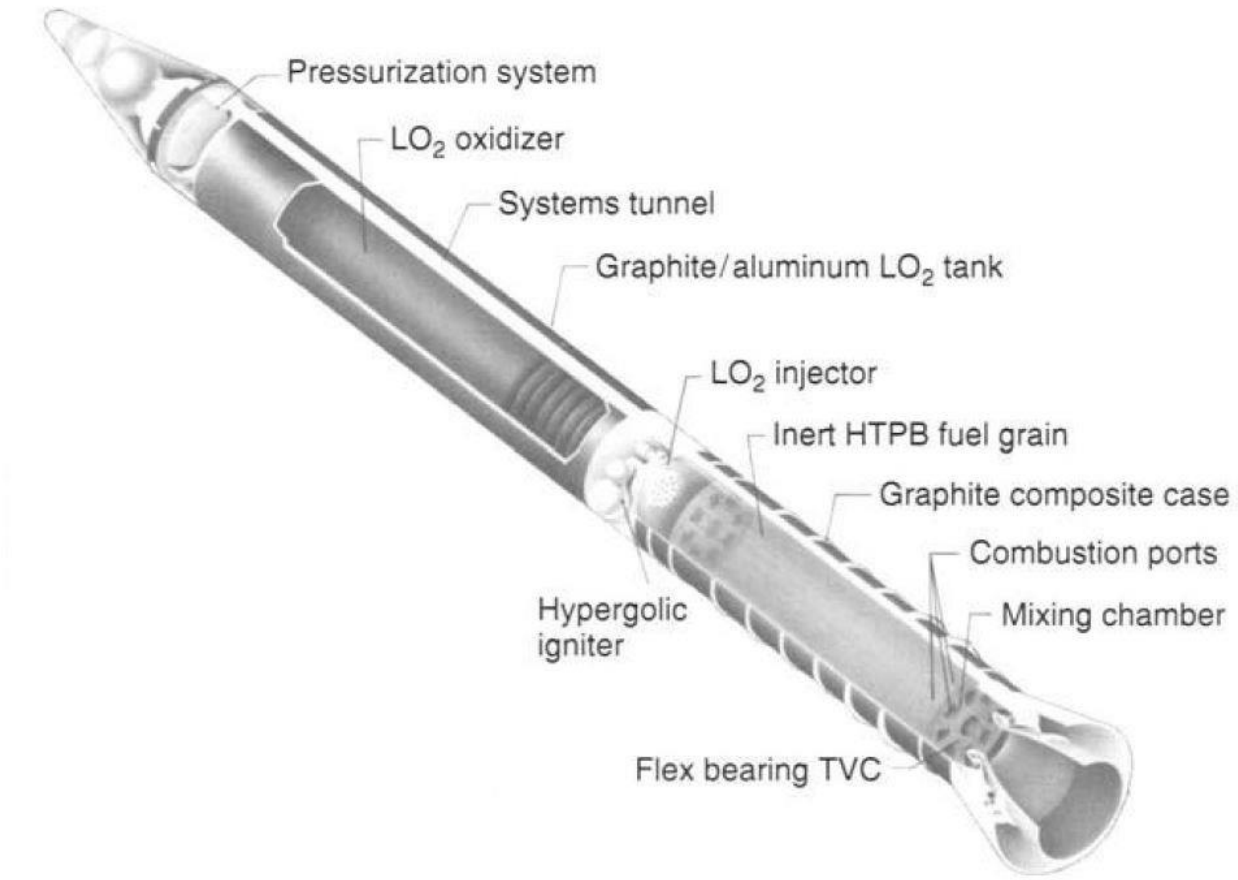

Figure 1.4: Typical Hybrid Rocket Configuration

Hybrid rockets are intrinsically more stable than liquid and solid propellant systems. For instance, the hybrid's solid fuel grain is completely inert, which reduces the risk of it detonating unintentionally during manufacturing or transportation. Liquid systems use energetic liquids and gases, such as hydrogen and methane for fuel, which are both explosive when exposed to atmospheric air. Solid rockets contain fuel combined with oxidizer as soon as they are manufactured, which means that sufficient energetic input or mishandling of the grain presents the potential for an explosion.

As previously alluded to, hybrid rockets are able to throttle their thrust similar to the way that liquid systems are able to accomplish this. This operation is simpler for hybrid

applications in that they only need to throttle the oxidizer flow, whereas liquid systems must throttle both the oxidizer and fuel systems. Furthermore, hybrid rockets do not suffer from the same combustion instabilities that liquid systems do [8], and offer a smooth transition of thrust across their entire throttling band. Similar to liquid systems, hybrids also boast the ability of being able to terminate their thrust simply by ceasing their oxidizer flow.

Hybrid rockets are also relatively easy to manufacture and ordinarily cheaper than their solid and liquid counterparts [8]. Since hybrid rockets throttle only the oxidizer flow, approximately half of the plumbing of a liquid system is required. Fuel grains for these systems are also easier to cast due to their less volatile nature when compared to solid rockets, requiring fewer safety precautions and regulations.

Unfortunately, hybrid rockets do suffer some drawbacks when compared to liquid and solid propellant systems. First and foremost is the low fuel grain regression rate, which is the speed at which the fuel burns normal to the fuel surface exposed to the oxidizer. The relatively low regression rate, leads to lower combustion efficiency and lower performance when compared to solid and liquid rocket engine configurations. In an industry where performance is vital and specific impulse (I_{sp}) is worth millions of dollars of development, this deficiency alone has relegated hybrid rocket motors to mostly research and hobbyist applications [9]. In addition to the low initial regression rate, the regression rate further decreases as the fuel grain port diameter increases, which causes the oxidizer to fuel (O/F) ratios to change as the hybrid motor continues to burn. This shift causes the I_{sp} of hybrid rocket motors to change unpredictably while in flight which can affect the mission profile.

1.4 Hydroxyl Ammonium Nitrate

The systems discussed in the previous sections all require oxidizer delivery to the fuel grain in order to function. Oxidizers include liquid or gaseous oxygen, to more exotic chemicals such as hydrogen peroxide or N_2O. Since the mission profile of some rockets, including missile interceptors, involve long periods of lying dormant before launch with little notice, chemicals that require a large amount of energy input, such as the cryogenic systems for LOX, quickly become infeasible. Hydroxyl Ammonium Nitrate (HAN) is a chemical that is used quite frequently as an oxidizer due to the fact that it is stable for long term storage, liquid at room temperature, non-corrosive, and relatively safe to handle. Some research has already been performed by Heister et al. [5] into using HAN as an oxidizer with a hydroxyl-terminated polybutadiene (HTPB) hybrid fuel grain, the results of which can be seen in Table 1.

Table 1.1: Experimental Data comparing various hybrid propellant combinations

Propellant Combination	Optimal O/F	ρ_f (g/cm^3)	ρ_{ox} (g/cm^3)	ρ_b (g/cm^3)	I_{sp} (s)	$\rho_b I_{sp}$ (g*s/cm^3)
LOX/HTPB	2.3	0.92	1.14	1.06	298.4	316
90% HP/PE	7.8	0.90	1.39	1.31	266.1	348
98% HP/PE	7	0.90	1.43	1.33	275.7	367
98% HP/DCPD	6.2	1.01	1.43	1.35	277.5	375
95% HAN/HTPB	9.6	0.92	1.68	1.56	251.1	392
N_2O/HTPB	7.4	0.92	1.98	1.74	266.4	463

1.5 AF-M315E Green Monopropellant

Currently, almost all of the operational monopropellant systems use hydrazine as their propellant due to its performance, maturity, and stability. Unfortunately, hydrazine is also extremely toxic, which has a multitude of other of other health hazards according to the National Institute for Occupational Safety and Health [6]. There has been a recent push by NASA and several private companies, such as Orbital ATK, Aerojet Rocketdyne, and Plasma Processes, to develop a replacement for hydrazine that has comparable performance but much lower toxicity than hydrazine. This effort, known as the Green Monopropellant Infusion Mission (GPIM), will culminate in the launch of a NASA/Ball Aerospace jointly developed satellite. This satellite will be propelled by an Air Force developed monopropellant known as AF-M315E, which has generated promising results, as highlighted in Table 2.

Table 1.2: A comparison of several GPIM propellants to hydrazine

Chemical	Density (g/mL)	Isp (sec)	Vapor Pressure @ 293 K (psia)
Hydrazine	1.01	230	0.203
Hydrogen Peroxide	1.45	165	0.097
LMP-103S	1.24	252	~
AF-M315E	1.46	266*	~

*Theoretical Isp

The Green Propellant Infusion Mission (GPIM) has launched a demonstration satellite to further mature the technology [7]. Due to the oxidizer rich nature that most systems run at, as well as some analysis done using NASA's CEA software (Appendix A), it is theorized that the decomposition products of AF-M315E will contain enough excess oxidizer to be able to ignite and sustain a combustion reaction with an HTPB fuel grain in a hybrid configuration. The eventual goal of this research endeavor is to eventually test this theory

using simulated AF-M315E decomposition gases as the oxidizer and HTPB as the fuel grain.

1.6 Project Relevance

Green monopropellants and hybrid rocket propulsion are two separate concepts, but approaching the problem from a system engineering standpoint, combining the two could methods potentially have a slew of benefits. Based on analysis done in NASA's Chemical Equilibrium with Applications (CEA) code [10], it is believed that after decomposing AF-M315E, there will be sufficient oxygen leftover in the form of CO_2, CO, NO, and NO_2 to sustain the combustion process of an HTPB hybrid fuel grain. After undergoing the decomposition process, these gases should be hot enough to self-ignite with the fuel grain, eliminating the need for a dedicated ignitor. Furthermore, the AF-M315E propellant can also be used with small thrusters to provide maneuvering capabilities. These capabilities make it perfect for Anti-Ballistic missiles, allowing for them to have a single, long-term storable propulsion system that does not require extensive power input or maintenance to remain mission ready. UTEP is currently under contract with the Missile Defense Agency to investigate the practicality of this type of system.

1.7 Project Objectives

The main objective of this project is not only to develop UTEP's ability to test a 250mm HTPB hybrid fuel grain, but more importantly to investigate the applicability of using green monopropellants as oxidizer gases with this fuel grain. In order to accomplish this goal, the system was designed and developed to test a medium scale hybrid engine (5lbf). A high-flow delivery system was developed in the bunker portion of UTEP's Goddard Propulsion Lab and was tested using the flow rates, grain adapter, and fuel grains with the first experiments performed to validate the experimental procedure. Next, the larger grain adapter and fuel grains were fabricated and tested with the HAN decomposition gases, including steam from a newly designed and developed steam generator, to form the baseline performance model, which is further detailed in later chapters of this report.

Chapter 2: Background and Theory

2.1 Regression Rate

Regression rate of a fuel grain is the rate at which the grain of the hybrid rocket regresses normal to the surface of the grain due to vaporization and subsequent combustion of the fuel contained therein [2]. This is one of the most important design parameters for hybrid and solid rocket motors, and is directly indicative of their performance. For solid rocket motors, the regression rate is a function of chamber pressure, as seen in Equation 2.1.

$$r = a * p_c^n \tag{2.1}$$

Where r is the regression rate, a is an empirical constant, p_c is chamber pressure, and n is the combustion index described by Sutton, et al. [2]. Combustion of the solid grain occurs directly on the surface of the grain, where the pre-mixed fuel and oxidizer react, causing an increase in pressure, which is directed through the nozzle to produce thrust. It should be apparent to the reader that the nature of this reaction and the resultant thrust is directly linked to chamber pressure. Hybrid rockets differ from this in that their regression rate at lower oxidizer flowrates is controlled by the mass flux of oxidizer flowing across the grain. In a hybrid rocket, the gaseous oxidizer is injected axially into the fuel grain, which creates a boundary layer on the fuel grain. When ignited, a flame layer forms inside of the boundary layer, as demonstrated in Figure 2.1.

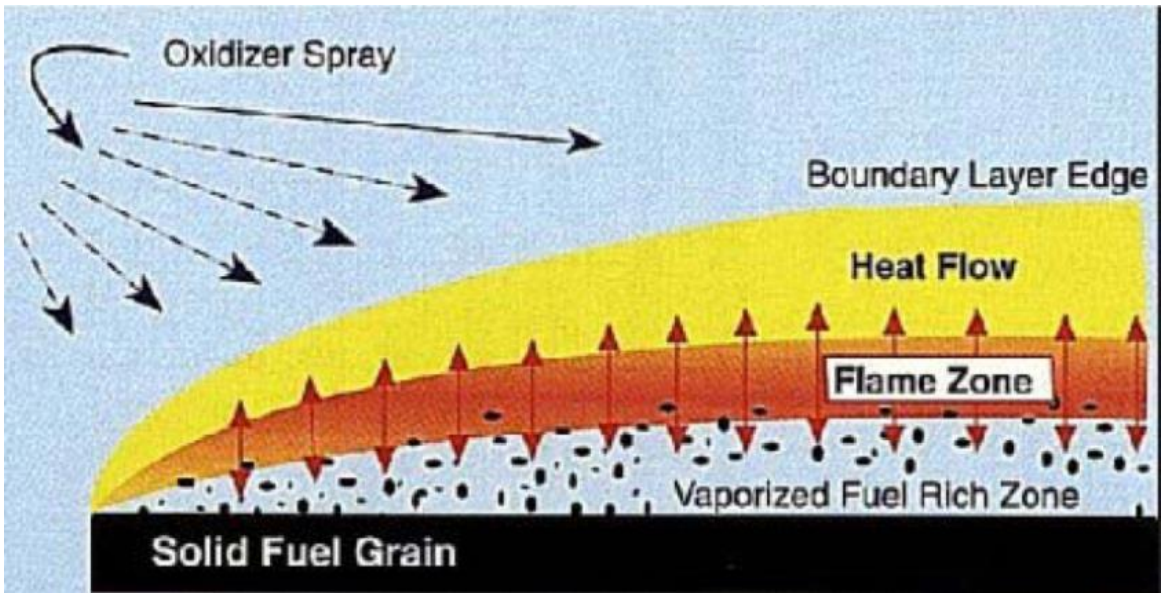

Figure 2.1: Depiction of the boundary layer that forms inside of hybrid fuel grains [11]

This flame is sustained by heat transferring into the fuel grain, creating a liquid or melt layer, with these liquid droplets absorbing more heat, causing them to vaporize before being ignited with the oxidizer.

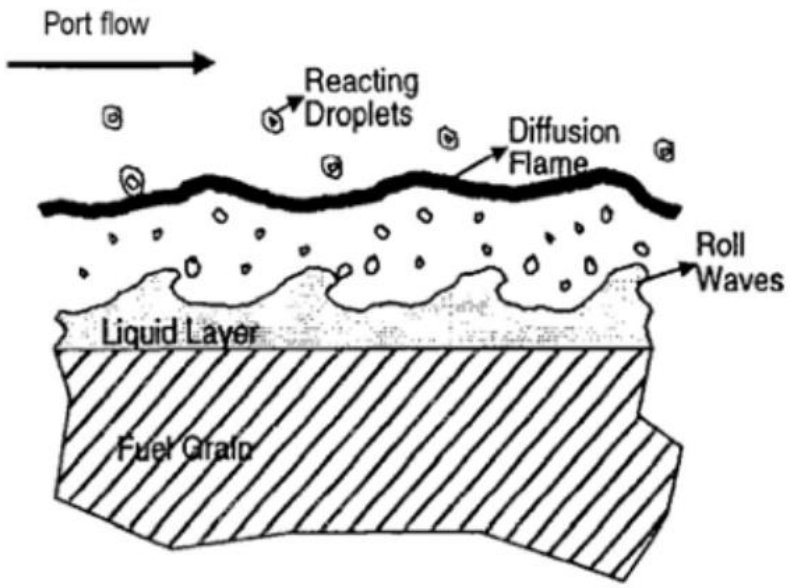

Figure 2.2: Demonstration of the fuel grain being liquified, then vaporized in a hybrid rocket motor [11]

Regression rate in hybrid motors is exceedingly difficult to precisely calculate due to the vast number of variables that have an effect on how the fuel regresses. One of the most groundbreaking studies in creating a simplified regression rate analysis was created by Marxman, et al. [12], which quantifies regression rate by analyzing the heat transfer in the turbulent boundary layer of a fuel grain. This analysis assumes that the boundary layer can be split into an oxidizer rich region above the diffusion flame and a fuel rich region below it, as seen previously in Figure 2.1. The fuel rich zone in this case is the region across which heat must flow in order to liquify and then vaporize the fuel grain, which means that the regression rate is proportional to heat flux. This relationship is described by Marxman [13] in Equation 2.2:

$$\rho_f \dot{r} = (\rho v)_w = \frac{\dot{Q}_w}{\Delta H} \tag{2.2}$$

Where ρ_f is the fuel density, $\dot{r}$ is the regression rate, $(\rho v)_w$ is the gas phase mass flux at the fuel surface, $\dot{Q}_w$ is the heat transfer per unit area to the fuel wall, and ΔH is the effective heat of gasification of the solid fuel. This theory was developed using a slab grain. However, this does not adequately represent the events occurring within the cylindrical motors most commonly used in pragmatic applications. Instead, most contemporary applications use an averaged regression rate law to determine the regression rate in their system, similar to the one in Equation 2.3 [14]:

$$\dot{r} = aG_{ox}^{n} \tag{2.3}$$

Where a is the regression rate coefficient, G_{ox} is the mass flux across the grain, and n is a propellant dependent constant. As previously mentioned, the mass flux dominated relationship in Equation 2.3 is only valid for lower oxidizer mass fluxes (<4.93 g/cm^2-s), such as those previously performed at UTEP [10]. Experimentation performed by Smoot et al. [15], and subsequently by Kuo et al. [16], show that as mass flux across the fuel grain increases, the regression rate of hybrid rocket motors becomes progressively more pressure dependent. There are three distinct regions of dependency on mass flux and pressure associated with hybrid rocket regression rate, as seen in Figure 2.3:

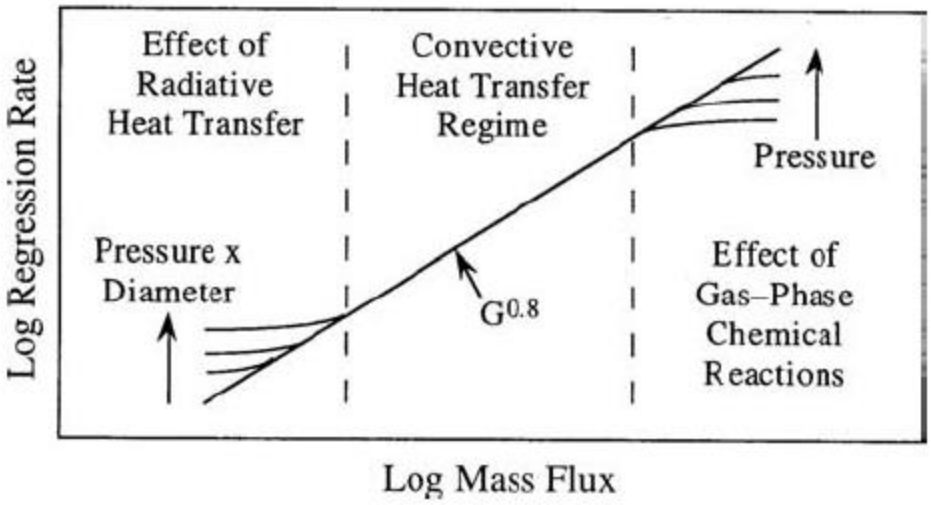

Figure 2.3: Regions of regression rate dependency [16]

Because of the effect that pressure has on regression rate in these higher regions, a new association was derived to describe the reactions happening during combustion [16]:

$$\dot{r} = \frac{aG^{0.8}bp^{n}}{aG^{0.8} + bp^{n}} \tag{2.4}$$

The current efforts for this thesis are focused on mass fluxes ranging from 5 to 10 g/cm^2-s, thus this analysis will be used when processing data on the fired fuel grains.

2.2 Regression Rate Improvement

The ultimate goal of this project is to improve the regression rate of HTPB with HAN, and later AF-M315E decomposition products. UTEP is looking at several methods to accomplish this, as listed here:

- Varying Channel Size/Geometry
- Advanced Injector Design
- Different Fuel Materials
- 3D Printed Fuel Grains

Varying the channel size or geometry is a common method of optimizing the regression rate of hybrid rockets to increase the amount of surface area that the grain has to burn. More interesting is the injectors which are specifically designed to improve regression rate. Currently still in preliminary development, the idea is that if the flow of oxidizer can be directed in a swirling pattern down the grain, it will increase the effective size of the grain and therefore increase the regression rate. Several designs have been conceived and prototyped with a Stratasys uPrint. Intensive development on these components will commence once the baseline testing has been completed. The first design is a simple pintle tip with a series of small holes that eject oxidizer radially, Figure 2.4.

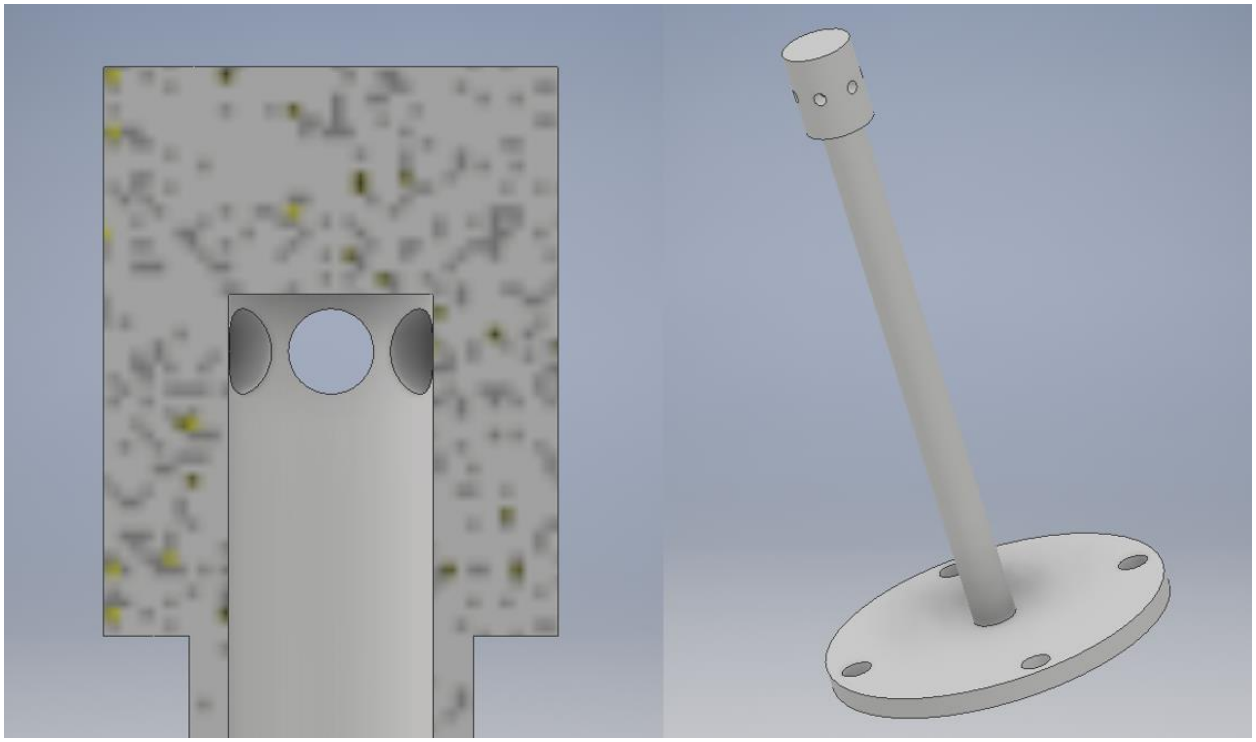

Figure 2.4: Conceptual pintle injector design that is placed inside of the fuel grain and used to inject oxidizer

The second design uses aspect from the co-axial swirl injector, which is further detailed in Chapter 3. This design consists of 4 tangential holes similar to the pintle design and a conceptual drawing of this type of injector can be seen in Figure 2.5.

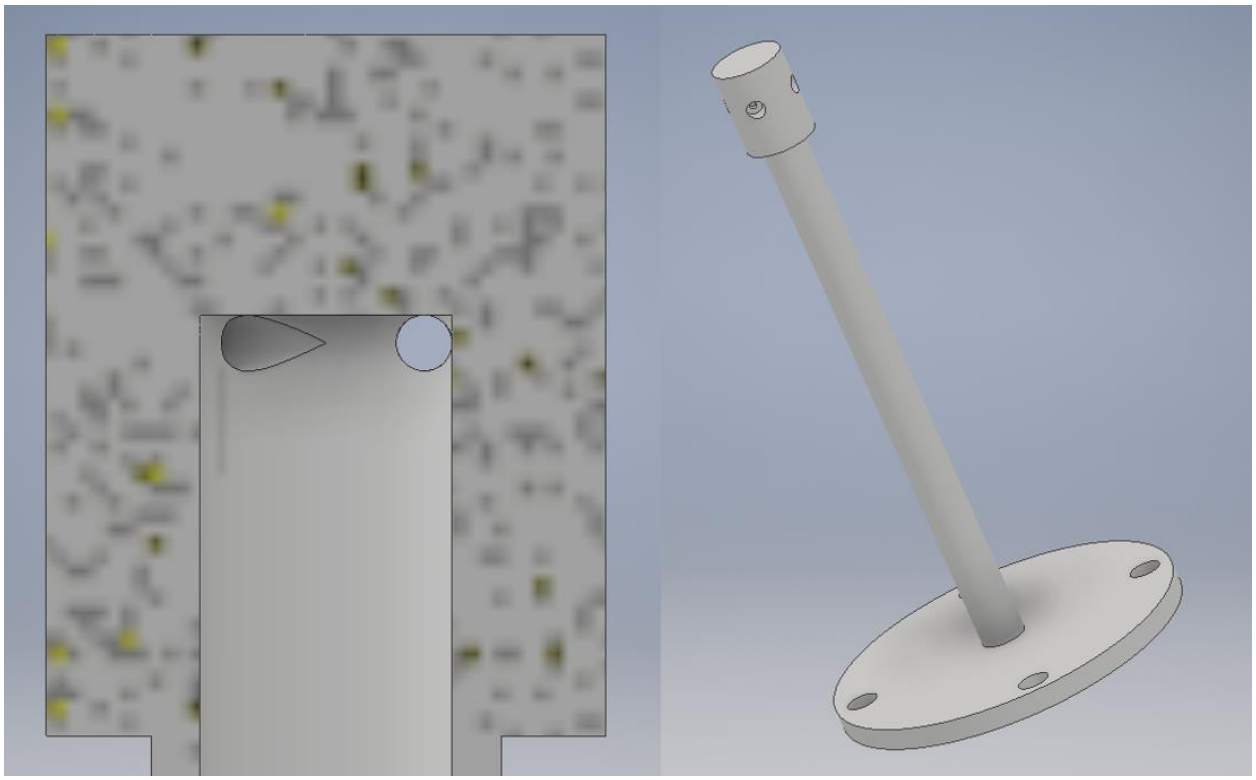

Figure 2.5: Conceptual co-axial swirl injector design that is placed inside of the fuel grain and used to inject oxidizer

Lastly, one of the most cutting-edge designs conceived is a dome shaped injector that will ideally begin to swirl the oxidizer upon its release from the injector and continue to swirl the oxidizer down the fuel grain channel. The design for this injector can be seen in Figure 2.6.

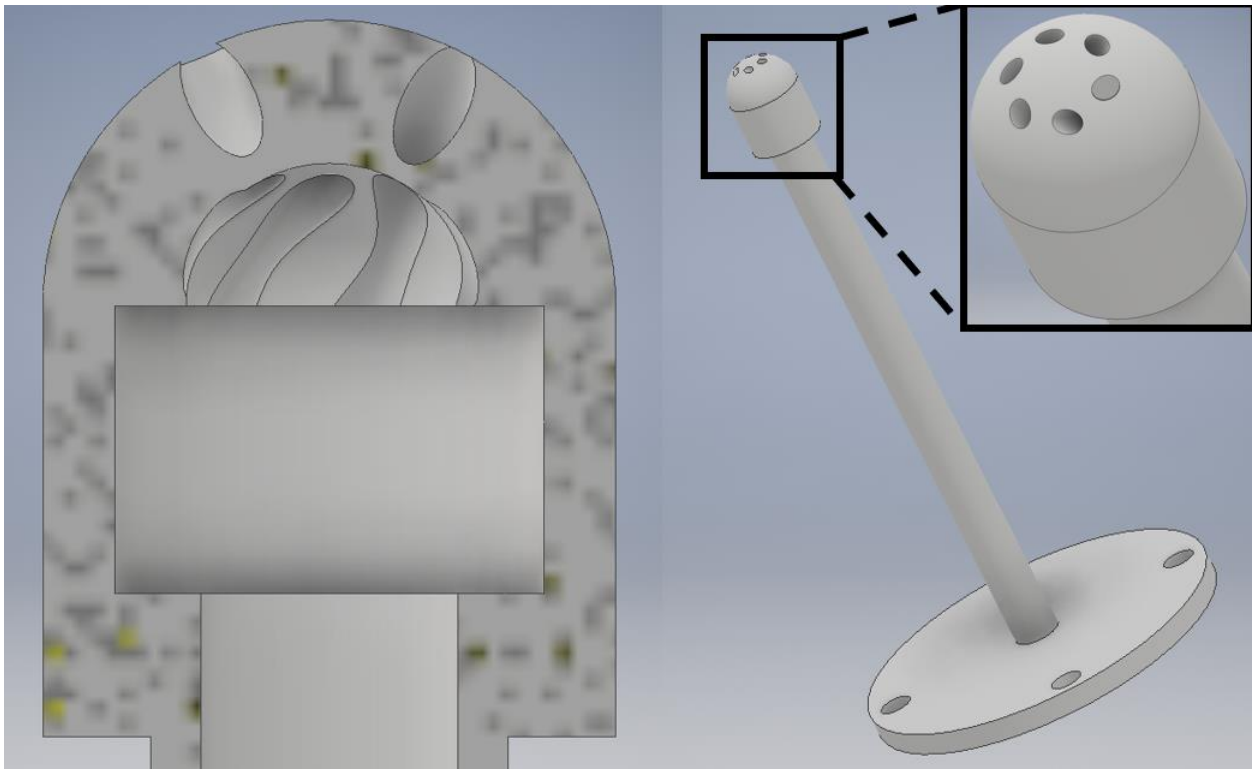

Figure 2.6: Conceptual swirl injector design that is placed inside of the fuel grain and used to inject oxidizer

While this project specifically uses HTPB as the fuel, some other fuel materials may be considered for use in combination with the aforementioned injectors. HTPB has become a mainstay of hybrid rockets due to its good mechanical properties and ease of manufacturing. In recent years however, research has been done on the development and use of new fuels. Table 2.1 shows a comparison of several different hybrid fuel/oxidizer combinations.

Table 2.1: Comparison of different hybrid Fuel/Oxidizer combinations [24]

Fuel	Oxidizer	Optimum O/F	Sea level I_{sp}, s	c^*, ft/s
HTPB	LOX	1.9	280	5972
PMM($C_5H_8O_2$)	LOX	1.5	259	5449
HTPB	N_2O	7.1	247	5264
HTPB	N_2O_4	3.5	258	5456
HTPB	RFNA	4.3	247	5219
HTPB	FLOX(OF_2)	3.3	314	6701
Li/LiH/HTPB	FLOX(OF_2)	2.8	326	6950
PE	LOX	2.5	279	5877
PE	N_2O	8.0	247	5248
Paraffin	LOX	2.5	281	5920
Paraffin	N_2O	8.0	248	5268
Paraffin	N_2O_4	4.0	259	5469
HTPB/Al(40%)	LOX	1.1	274	5766
HTPB/Al(40%)	N_2O	3.5	252	5370
HTPB/Al(40%)	N_2O_4	1.7	261	5509
HTPB/Al(60%)	FLOX(OF_2)	2.5	312	6582
Cellulose ($C_6H_{10}O_5$)	GOX	1.0	247	5159
Carbon	Air	11.3	184	4017
Carbon	LOX	1.9	249	5245
Carbon	N_2O	6.3	236	4992
	Cryogenic hybrids			
Pentane(s)	LOX	2.7	279	5870
CH_4(s)	LOX	3.0	291	6140
CH_4(s)/Be(36%)	LOX	1.3	306	6292
NH_3(s)/Be(26%)	LOX	0.47	307	6452
	Reverse hybrids			
JP-4	AN	17.0	216	4651
JP-4	AP	9.1	235	5007
JP-4	NP	3.6	259	5476

It can be seen that paraffin wax has performance that is comparable to HTPB and also has a higher regression rate [25]. HTPB is a rubber-like substance that requires an intense heat to melt and mix with the oxidizer. In addition, HTPB also requires a relatively long manufacturing process, as detailed in Appendix B. An additional advantage of paraffin is

that it can simply be heated to its melting point and recast into whatever shape is desired. Paraffin attributes also lend well to the additive manufacturing process, material extrusion, where material is drawn through a nozzle, then heated and is finally deposited layer by layer [27]. This process has been experimented with, and shows promising results for easily manufacturing grains in the future [26]. Thus, paraffin may be considered in future designs similar to those presented in this thesis.

2.3 HAN Decomposition

It is known that hydroxyl ammonium nitrate (HAN), is one of the major components of AF-M315E [20]. HAN is storable as a stable liquid when mixed with water, but in order to use it as an oxidizer it must be decomposed, either thermally or catalytically. Thermal decomposition is achieved by heating the sample until decomposition has occurred, whereas catalytic decomposition involves heating a catalyst, typically a transition metal such as silver, platinum, or iridium, to a certain temperature and having the HAN sample come into contact with it. Courthéoux et al. published two papers [17,18] describing their research into the decomposition of HAN. They heated several samples of varying dilutions in a batch reactor and used thermogravimetric analysis and differential thermal analysis to ascertain parameters intrinsic to the decomposition of HAN, such as its concentration at decomposition, the onset temperature of decomposition, and its exothermic peak. As one would expect, the results differed between the two different decomposition methods for a 40% HAN solution with thermal decomposition occurring at 135°C, and catalytic decomposition transpiring at 107°C with a platinum catalyst, as seen in Figures 2.7 and 2.8, respectively.

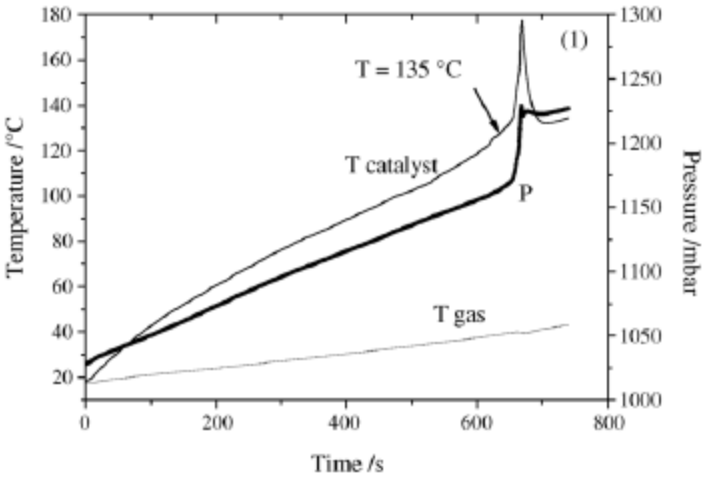

Figure 2.7: Thermal decomposition of 40% HAN solution [17]

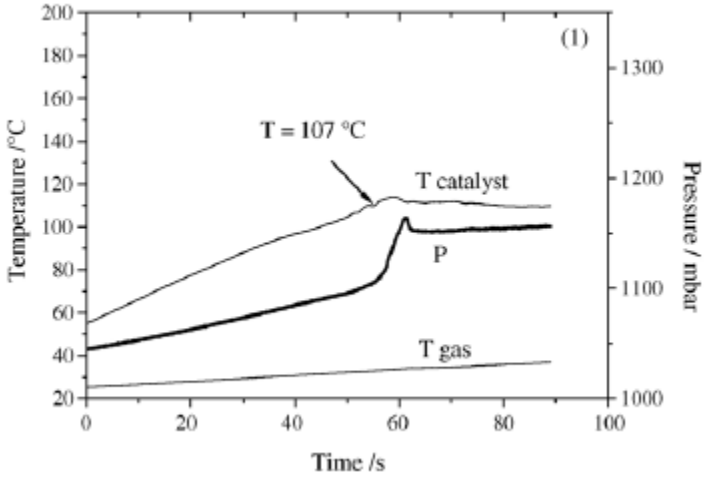

Figure 2.8: Catalytic decomposition of 40% HAN solution [17]

More recent studies into the decomposition of HAN have focused on the decomposition products resultant from the different methods of decomposition. A study by Chambreau [19] revealed that thermal decomposition produces different products than catalytic decomposition. Furthermore, decomposition products vary depending on the material used for the catalyst. Figure 2.9 compares the decomposition products of copper and iridium at different photo ion currents and temperatures.

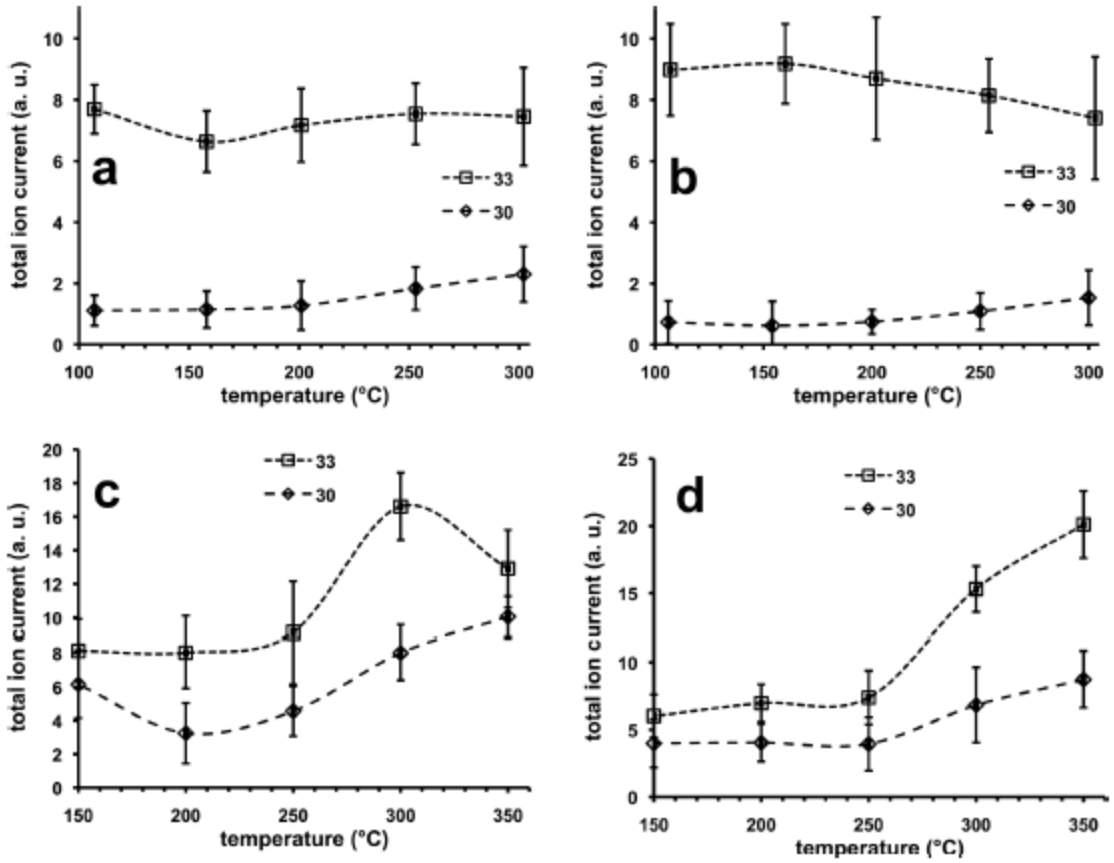

Figure 2.9: Integrated photo-ion signals as a function of temperature for m/z 30 (nitric oxide) and m/z 33 (hyaluronic acid) on (a) copper 8.5-10.5 eV (b) copper 11.5-14.5 eV (c) iridium 8.5-10.5 eV (d) iridium 11.5-14.5 eV

Lastly, an analysis was conducted at UTEP using NASA's Chemical Equilibrium with Applications (CEA) code [10], which can be seen in Appendix A. For the input, a 95% HAN solution was chosen as the oxidizer and yielded the results presented in Table 2.2:

Table 2.2: Results of the analysis of HAN decomposition using NASA's CEA code

Species	Formula	Mass Fraction
Oxygen	O_2	0.29591
Nitrogen	N_2	0.26957
Steam	H_2O	0.38657
Nitric Oxide	NO	0.01610

As previously stated, HAN is present in AF-M315E and is the main oxidizer of the monopropellant. Generally, rocket engines are run oxidizer rich which means that they have an excess of oxidizer when the reaction is completed. Assuming that this is the case with AF-M315E, it means that there is a good chance that there will be enough excess oxygen left to burn a hybrid fuel grain after the propellant has been decomposed.

2.4 AF-M315E

The composition of AF-M315E propellant is not widely known due to its proprietary nature. However, there are a few things that can be inferred about its chemical makeup from experiments performed at UTEP. HAN represents the oxidizer portion of the mixture, used in conjunction with an unknown fuel component. It is assumed that there is some amount of water in the mixture as well to increase the stability of the propellant for long term storage and transportation. Research is currently ongoing at UTEP to determine the decomposition products of AF-M315E so that it can be determined if there are enough oxidizer components available after the catalytic decomposition to sustain the combustion process in a hybrid rocket. It is feasible that the products of HAN solution decomposition could be used to increase the amount of oxidizer leaving the catalyst bed.

One of the most attractive features of using AF-M315E is that its decomposition temperature is high enough (1600 to 1800°C) that the system may not need a dedicated ignitor to initiate combustion of the fuel grain. In addition to providing the main thrust for the vehicle, the propellant can also be used in a monopropellant configuration to provide reaction control for the vehicle, all using a common fuel tank, reducing the weight and overall complexity of the vehicle. Comparable efforts have been made in an attempt to exploit similar green monopropellants and increase their potential in different aspects of spacecraft and vehicle propulsion [28].

Chapter 3: Experimental Methodology

3.1 Experimental Setup

3.1.1 Low Flow Test Setup

Previously, a low flow test system was built as a bench test at UTEP to validate several aspects of the project before building a higher flow system to perform research [10]. Among the elements looked at with the low flow system were:

- Ability to accurately measure regression rate
- Ability to mix oxidizer gases and steam
- Ability to create HTPB fuel grains
- Verify operation and control methods
- Verify ignition system

The basic design of the system is to allow for oxidizer gases to flow from K-bottles through a feed system into a specialized component designed to contain the fuel grain known as the grain adapter. Figure 3.1 contains a schematic of the low flow system and Figure 3.2 shows a picture of the system.

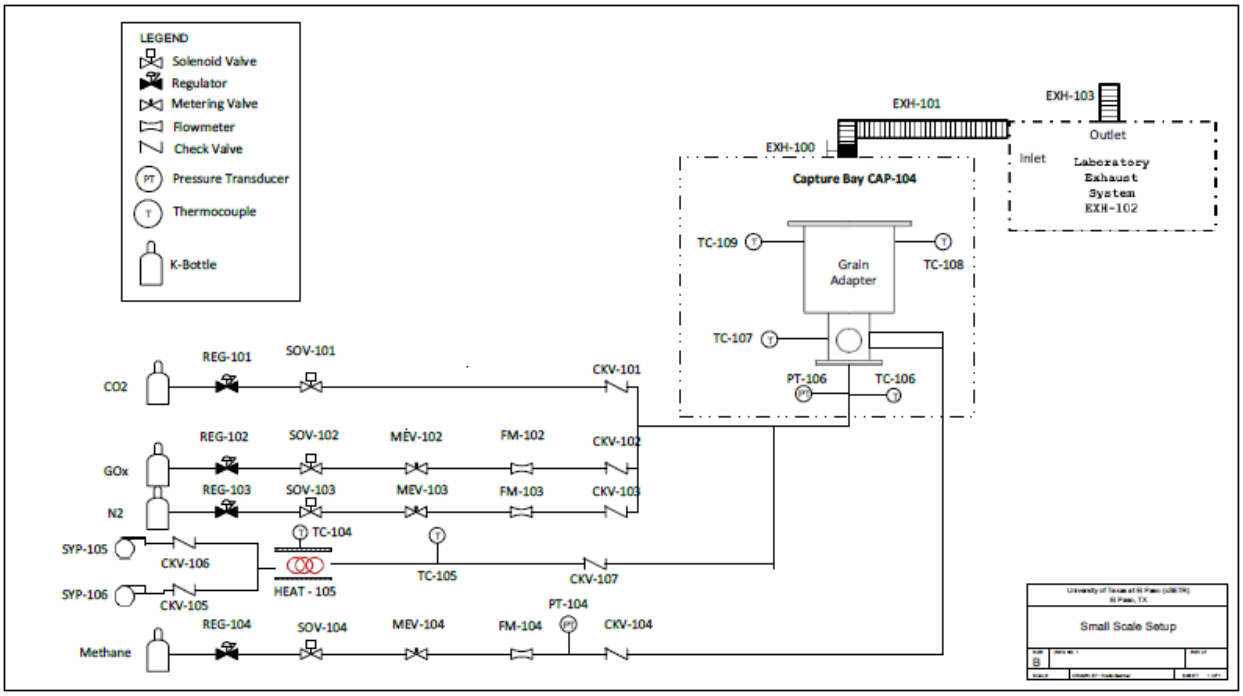

Figure 3.1: Schematic diagram of the low flow system [10]

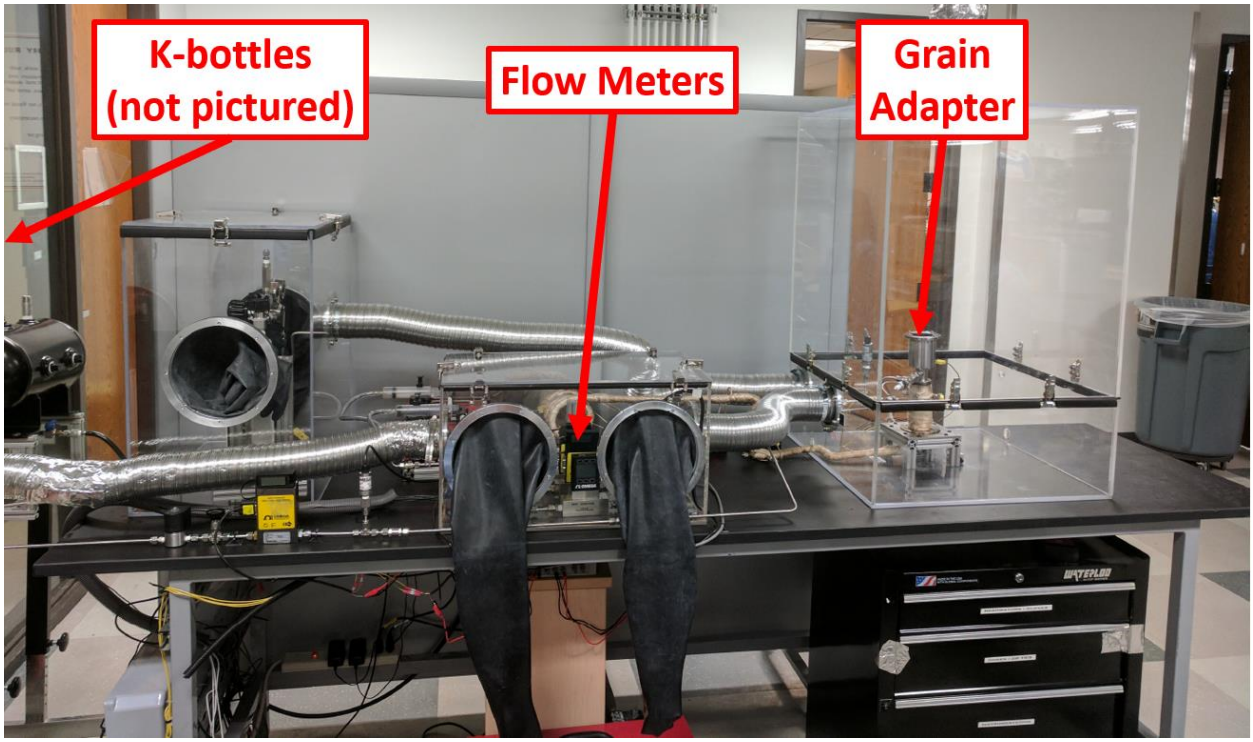

Figure 3.2: Picture of the low flow system

The system was used for testing of several GOX and HTPB mixtures, results shown in Section 4 of this thesis. Other attempts were also made with this system with HAN Decomposition Products and HTPB. From this system there were several lessons learned which helped to shape the development of the system presented in this thesis, the high flow system, listed here:

- The steam generator did not produce super-heated steam, which led to steam condensing on the fuel grain and prevented it from igniting
- The internal ignition system was problematic, so an external system was developed

3.1.2 High Flow System Design

For this system, in addition to wanting to increase the mass flux across the fuel grain, it was desirable to increase the length of the fuel grain so that the system represents conditions similar to published literature. From the outset, the intention of the project was

to eventually build the system inside of the bunker in UTEP's Goddard Propulsion laboratory. Lessons learned from the low flow system are used to complete the design to accomplish the project's remaining goals.

3.1.3 Delivery System

Previously, a delivery system was built with the goal of testing several different propulsion systems. This would allow for the rapid interchange of test articles to minimize time between tests and maximize the utilization of resources. For this project, prior to testing this system was redesigned and rebuilt to operate more efficiently and meet the needs of the current investigation.

System design is complicated, from initial concept to testing, and needs to be adjusted, optimized, and calibrated based on design requirements and to obtain optimal data acquisition. The delivery system presented in this thesis underwent a dozen configurations, which were evaluated and modified before finally deciding on the final design seen in Figure 3.3. This design was chosen as the final iteration because of the reliability and redundancy it provides, plus it allowed the team flexibility for other testing that is simultaneously ongoing.

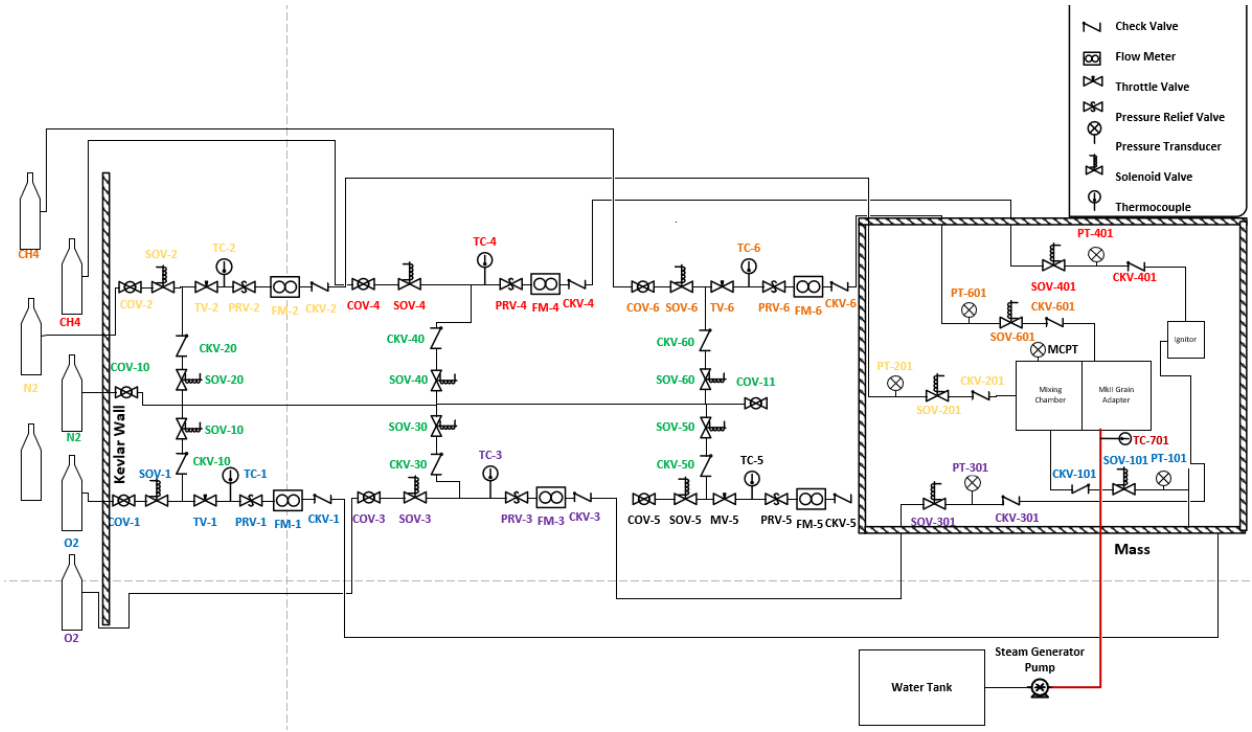

Figure 3.3: Delivery System Schematic

Each of the lines in Figure 3.3 has the ability to measure flowrate, pressure, and temperature via the flowmeters, pressure transducers, and thermocouples, respectively. The variations in the lines come from their specific purpose in the system. For instance, lines three and four supply the ignitor. Previous testing of the ignitor has proven that the line length between the final valve (valves 301 and 401) needs to be minimized in order to achieve optimal performance of the igniter, which is why the check valves were relocated upstream of the valves, as opposed to normal design convention. This design decision was compensated for by well-documented procedures and literature so that future generations of students would understand why these decisions were made. Table XXX contains a component list for the system.

Table 3.1: Delivery System Component List

Part Description	Number in System	Manufacturer	Part #
Cut-Out Valve	6	Swagelok	SS-4P4T-BK
Normally Closed Solenoid Operated Valve	6	Parker	71215
Normally Open Solenoid Operated Valve	12	Parker	71295
Throttle Valve	4	Deltrol	EN20 S
K-Type Thermocouple	6	Omega	5SRTC-TT-T-24-36
Relief Valve	6	Omega	SS-4R3A
Flowmeter (0-200 SLPM)	2	Omega	FMA1843A-ST
Flowmeter (0-50 SLPM)	2	Omega	FMA1828A-ST
Check Valves	12	Swagelok	H400SS 1/4
Pressure Transducers	7	Omega	PX302-500GV

Many special features were incorporated into the design for safety and ease of operation as well. A good example of this is the valves used in the system, which were specifically chosen based on their default orientation. Using line one as an example, SOV-1 is normally closed, while SOV-10 and SOV-101 are normally open. By having the valves set up like this, upon a complete loss of power, the oxidizer gases will be secured while the purge gases will be allowed to flow freely. This will allow for the system to purge and can be secured by shutting COV-10 once the area is deemed safe. Further details on the system and its operation can be seen in section 3.5 of this document, as well as the Test Procedure located in Appendix B.

3.1.4 Steam Generating System

As previously mentioned, the steam generating system required redesign before attempting to test. For this purpose, analysis was performed to determine the minimum length required to super heat the steam. This was done using heat transfer equations, including Equation 3.1, which describes heat transfer into liquid water. Solving for temperature in Equation 3.1 reveals the length of heated tubing necessary to heat water to its saturation point.

$$L_1 = \frac{\dot{m} c_p (T_f - T_i)}{h 2\pi r_i (T_s - T_\infty)} = 0.74\ m \tag{3.1}$$

Where L_1 is length of the tube to heat water to its saturation point, $\dot{m}$ is mass flow rate, c_p is specific heat value of water, h is the heat transfer coefficient, r_i is inner radius, T_f is final temperature, T_i is initial temperature, T_s is the setpoint temperature of the heating coil, and T_∞ is the ambient temperature. Plugging values into this formula yielded a critical length of 0.74 m for the water pumped into the system to reach saturation temperature. A second length calculation was implemented to calculate the length of tubing required to vaporize the water, Equation 3.2.

$$L_2 = \frac{\dot{m} h_{fg}}{h 2\pi r_i (T_s - T_\infty)} = 10.45\ m \tag{3.2}$$

Where L_2 is the length of tubing required to vaporize the water and h_{fg} is enthalpy. Solving this value resulted in a length of 10.45 m, which was combined with L_1 to have a total length of 11.19 meters to achieve a minimum heated length for superheated vapor. Continuing this analysis, calculations to determine the final temperature of the superheated steam were conducted as seen in Equation 3.3.

$$T_e = \frac{L_3 h 2\pi r_i (T_s - T_\infty)}{\dot{m} C_p} + T_i \tag{3.3}$$

Where T_e is exit temperature, L_3 is the superheating length, and T_i is the initial temperature. Using L_3 as a variable, a chart was generated to show the increase in steam temperature as a function of length, seen in Figure 3.4.

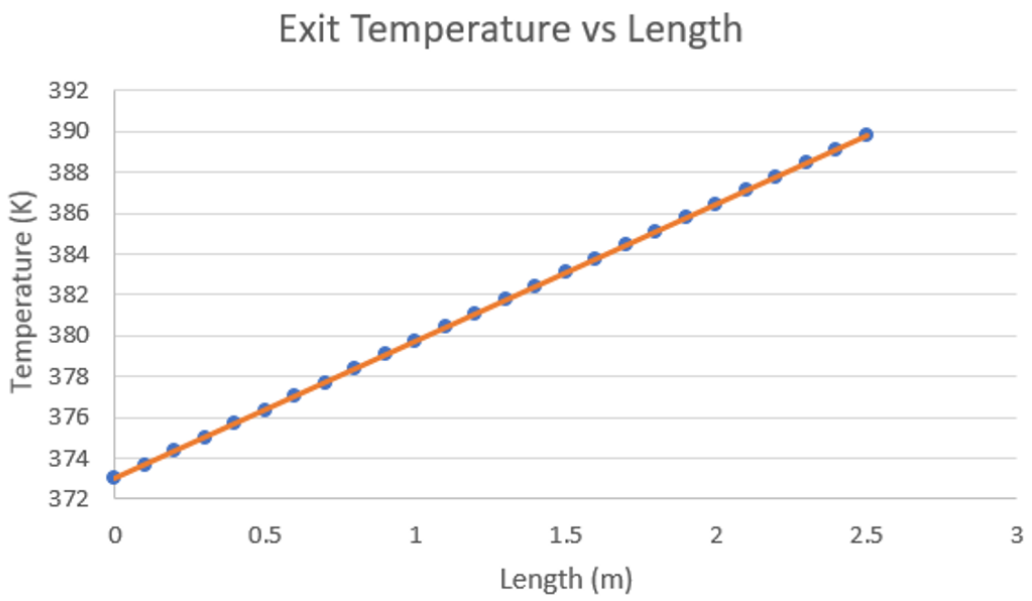

Figure 3.4: Exit Temperature of Steam from the Steam Generator as a function of Tube Length

In constructing the updated steam generator, it was decided to make the heated length as long as possible to superheat the steam. Thirty-six feet (18.29 m) of tubing was coiled and wrapped with heat rope in order to construct the heated portion of the steam generator. The water is delivered to the system via a pair of syringe pumps which are set up in parallel to provide a constant, set flowrate of water into the system. A schematic of the steam generating system has been provided in Figure 3.5.

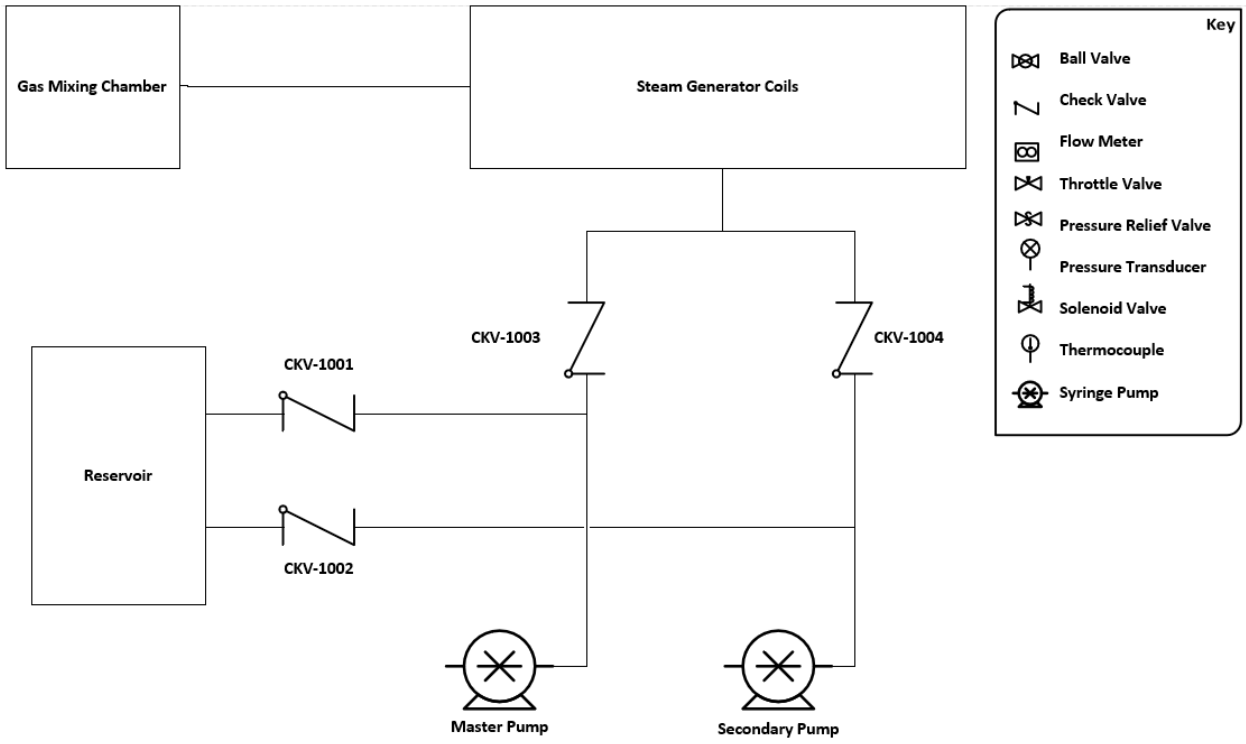

Figure 3.5: Steam Generator System Schematic

With this heated length, as well as preheating the components that the steam will come into contact with, the system is significantly more robust than previous iterations of steam generators that were used during small scale testing [10]. The length of heated tubing used should yield a superheated steam temperature of approximately 421K.

3.1.5 Methane Igniter

In order to initially ignite the system, the following design parameters were first considered:

- Internally Mounted Methane Ignitor
- Externally Mounted Methane Ignitor
- Solid Propellant “Squib”
- Internal Spark plug with methane flow

Ultimately, it was decided to keep the system consistent with methods that have proven successful with the previous small-scale system. In the small-scale system a handheld igniter was used exterior to the system in order to ignite a methane diffusion flame. Thus, an eternally mounted methane igniter is used. However, due to the significantly higher flowrates being used, a previously patented methane/GOX igniter is used. The igniter is operated remotely from a control room adjacent to the test section presented in Figure 3.3. The igniters provide a very hot (~3500K) burst of energy sufficient to ignite a methane diffusion flame which provides the heat necessary to initiate combustion in the hybrid fuel grain. Figure 3.6 is a picture of several of the ignitors that UTEP has manufactured. Figure 3.7 is an engineering diagram of the ignitor.

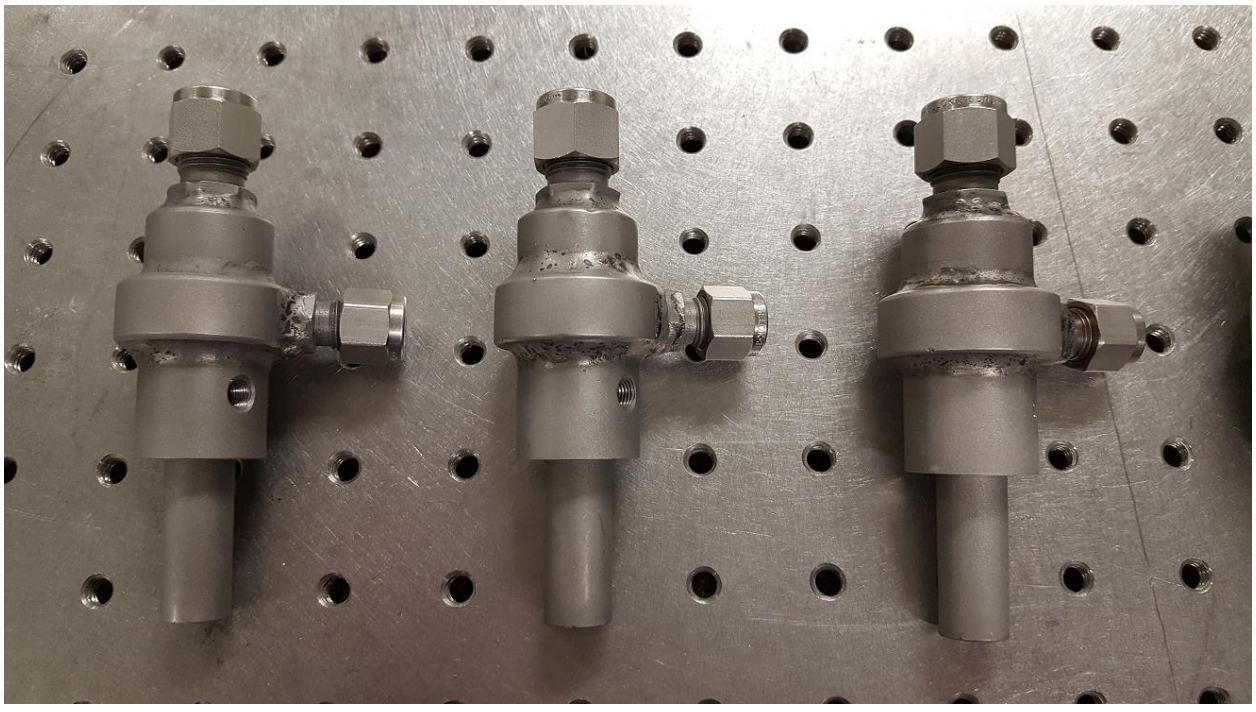

Figure 3.6: UTEP's Patented CH4/GOX Ignitors

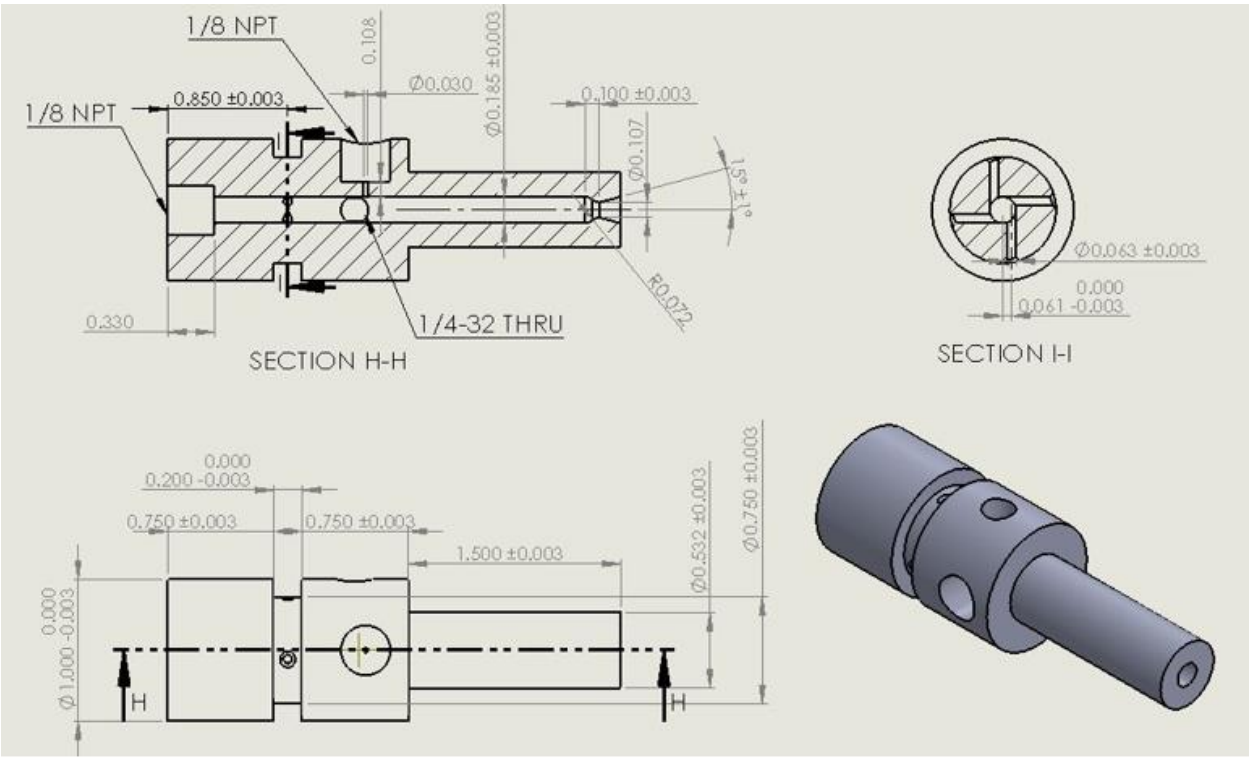

Figure 3.7: Engineer Diagram of UTEP's Patented CH4/GOX Ignitor [21]

3.2 Test Article

Once the delivery system has directed gases into the test section, the gases flow into the test article, which are a combination of a gas mixing chamber, injector, and a grain adapter. The general flow of gases through the test article can be seen in Figure 3.8.

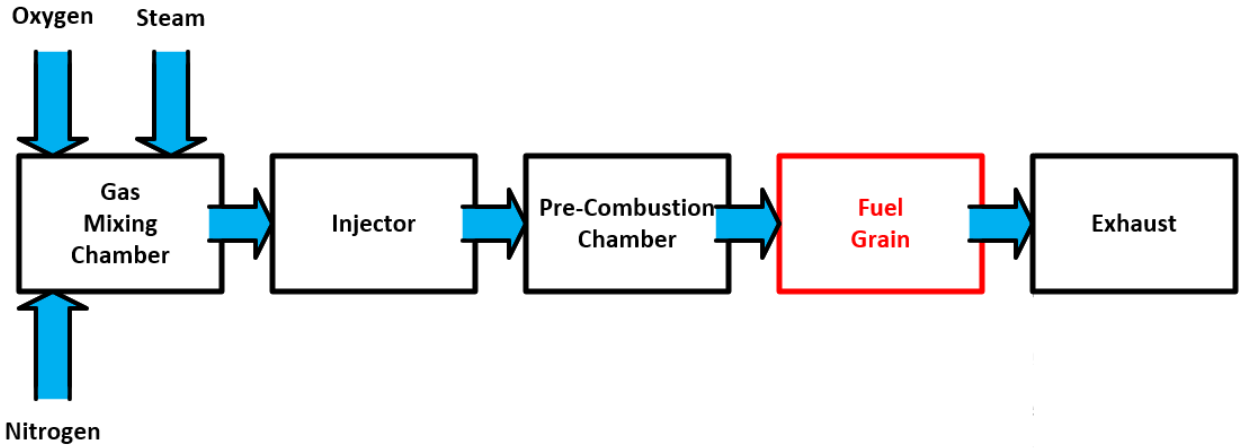

Figure 3.8: Block Diagram of the Test Article

3.2.1 Gas Mixing Chamber

Since the system was being designed and built, certain design requirements were met. The Gas Mixing Chamber is one component that is initially designed, with the following design requirements:

- Ability to mix at least 4 gases
    - Rated up to 450 psi
    - Two gas lines are able to sample at 200 Liters Per Minute (LPM) and two others are capable of 50 LPM
- Long enough for the gases to mix homogenously
- Ability to sample pressure up to 200 psi?
- Able to easily adapt to current and future grain adapter designs

Working within these parameters, several designs were conceived with their own advantages and disadvantages. All of these designs feature a 10-inch barrel shaped section, which, according to Cengal [23], allows for gases to mix homogenously if sufficiently long. The first of these designs considered was simply four small tubes flowing axially into a larger section where they mix before going into the injector, Figure 3.9.

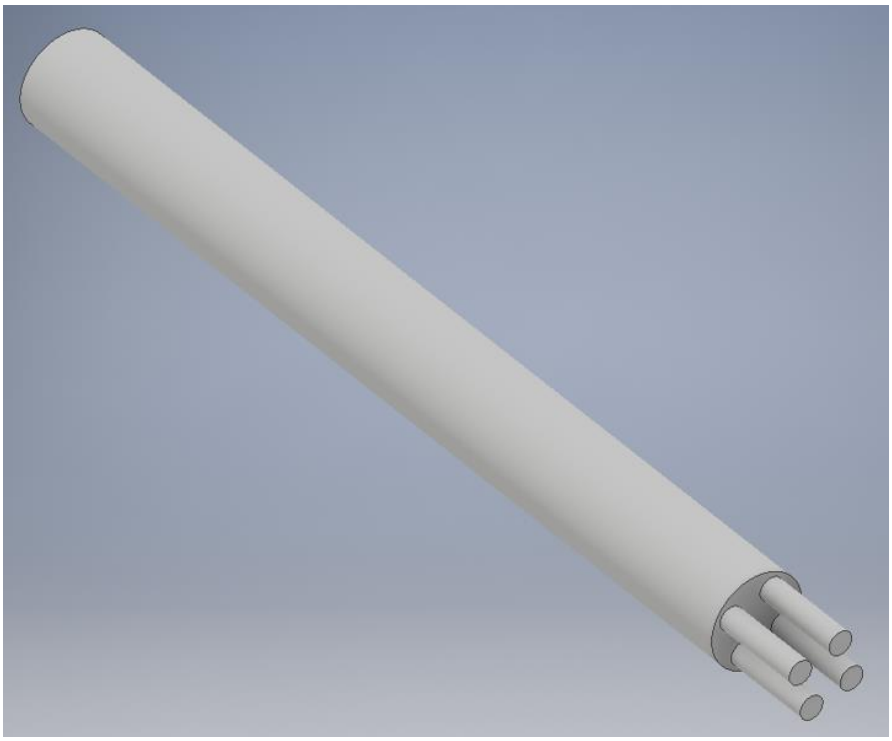

Figure 3.9: Inline Port Gas Mixing Chamber

This design was not selected due to the tight tolerances needed on the interface between the inlet tubes and the barrel section. This would be problematic not only for welding all of the tubes into the interface, but also for being able to tighten the fittings due to the tight clearances. This led to the second design iteration. The second iteration uses tangential gas mixing inlets into the chamber. This chamber has tubes entering the barrel section radially at a slight offset so that the gases swirl around the edges of the chamber to increase the effectiveness of the mixing process. This design is pictured in Figure 3.10.

Figure 3.10: Tangential Gas Mixing Chamber

Lastly, after some research, an interesting design was found previously used for medical applications. In this case, it's a device developed for microfluidic applications by Chen, et al. [22]. This device was scaled up and integrated into the barrel section in order to adapt it to the system, and is pictured in Figure 3.11, with a cross-sectional image of the swirl section in Figure 3.12.

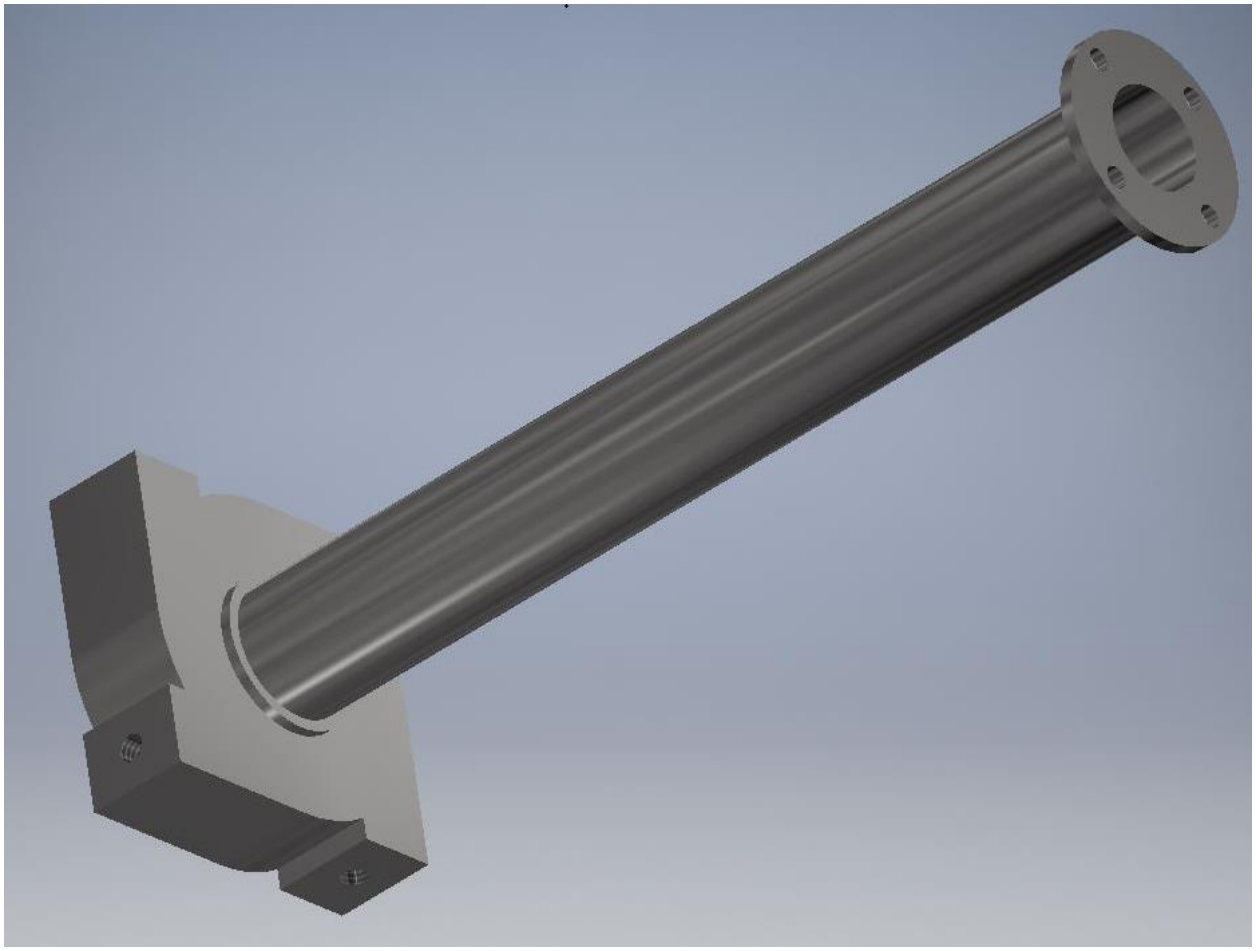

Figure 3.11: Swirl Gas Mixing Chamber

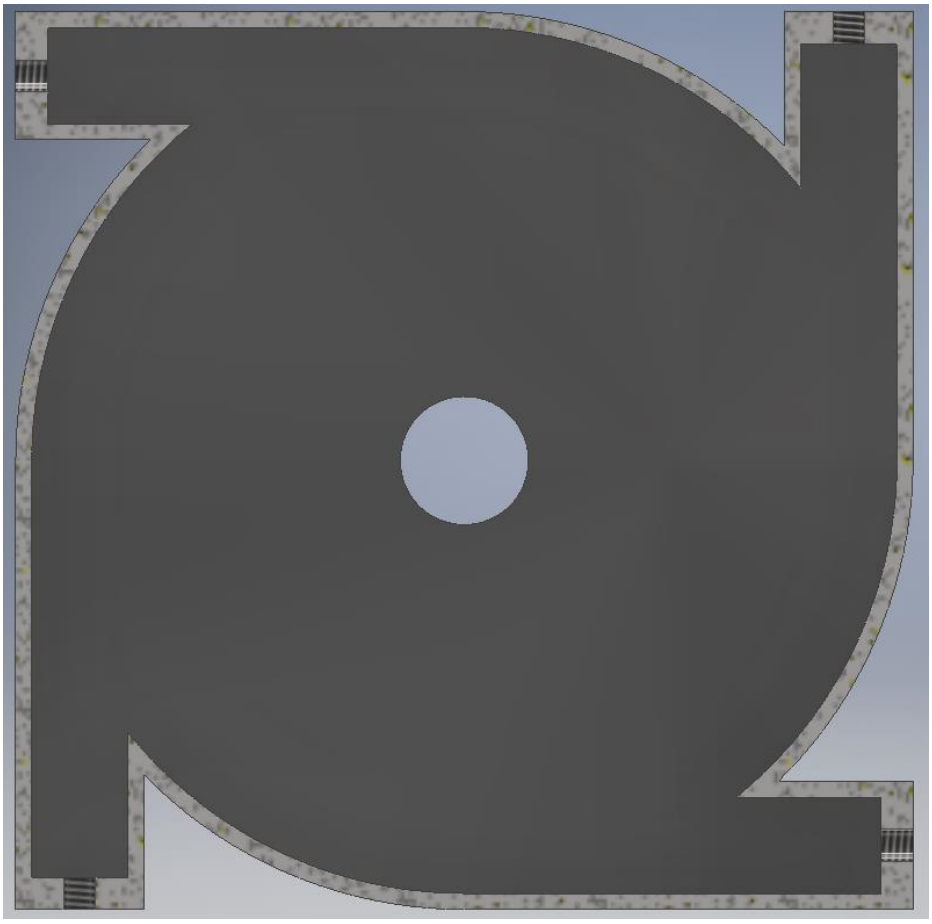

Figure 3.12: Gas Swirl Mixing Chamber Cross-Section View

The swirl and tangential Gas Mixing Chambers presented great potential for development, so manufacturing options were assessed to see which would present the most economical decision for development. Due to the complicated geometries of the swirl mixing chamber, 3D Printing emerged as the most viable option for having it manufactured. Unfortunately, the cost of having the swirl mixing chamber manufactured via 3D Printing proved prohibitively expensive. The tangential mixing chamber was manufactured in-house, Figure 3.13.

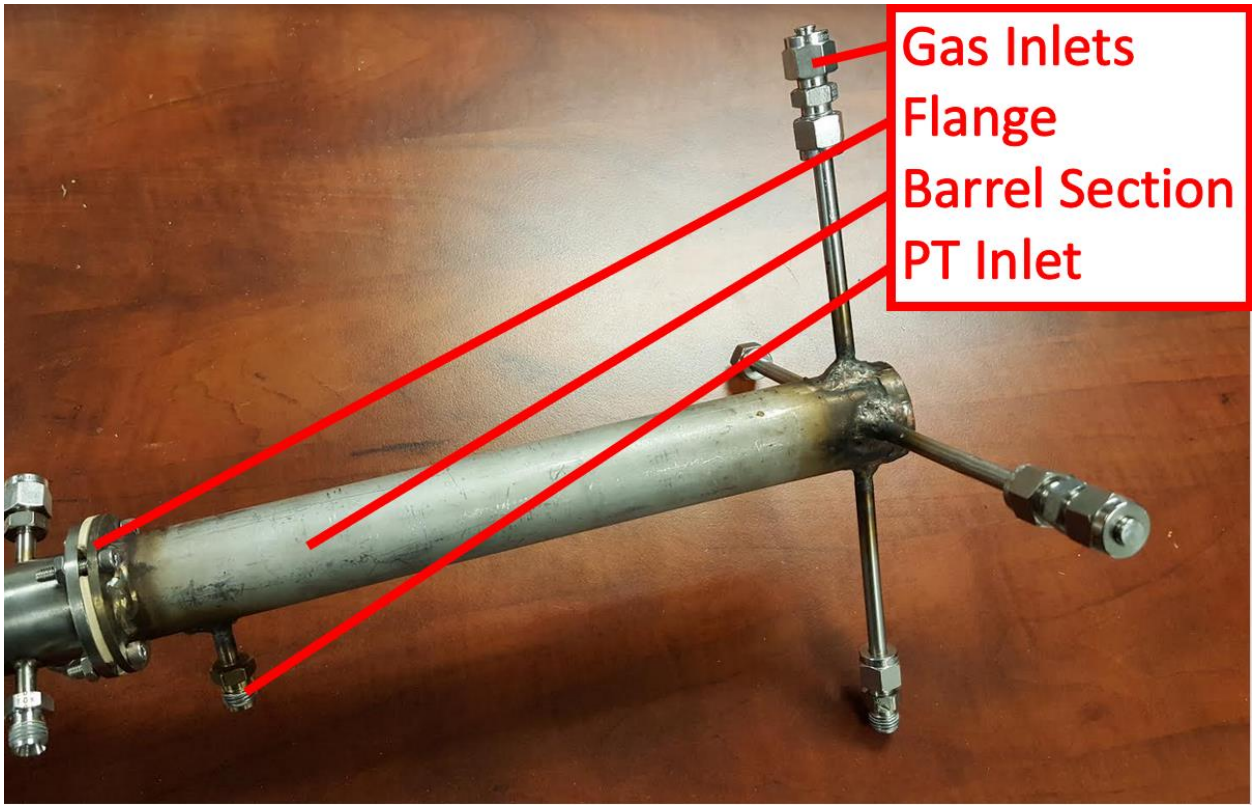

Figure 3.13: Fabricated Tangential Gas Mixing Chamber

The end flange on the gas mixing chamber was specifically designed so that it was able to adapt to the existing low flow grain adapter. While manufacturing the gas mixing chamber, a connection to that flange was generated so that it would be able to easily adapt to the yet to be manufactured high flow grain adapter, which fulfills the final design requirement initially set for the gas mixing chamber.

3.2.2 Grain Adapter

The high flow grain adapter was designed to meet the requirement of having a modular design compared to iterations. Specifically, the following design requirements were implemented:

- Increase the length of the fuel grain from 50mm to 250mm.

- Implementation of a pre-combustion chamber so that the entire upstream face of the grain is exposed to the oxidizer. The low flow fuel grain did not include this feature and it is believed that it may have affected the way the fuel grain combusted.
- The low flow grain adapter also lacked instrumentation ports on the throat to measure pressure, so it is desirable to include at least two ports on the throat of the high flow grain adapter.
- Ability to adapt to the gas mixing chamber.

Bearing these requirements in mind, the design of the high flow grain adapter materialized as the version shown in Figure 3.14 as an exploded view.

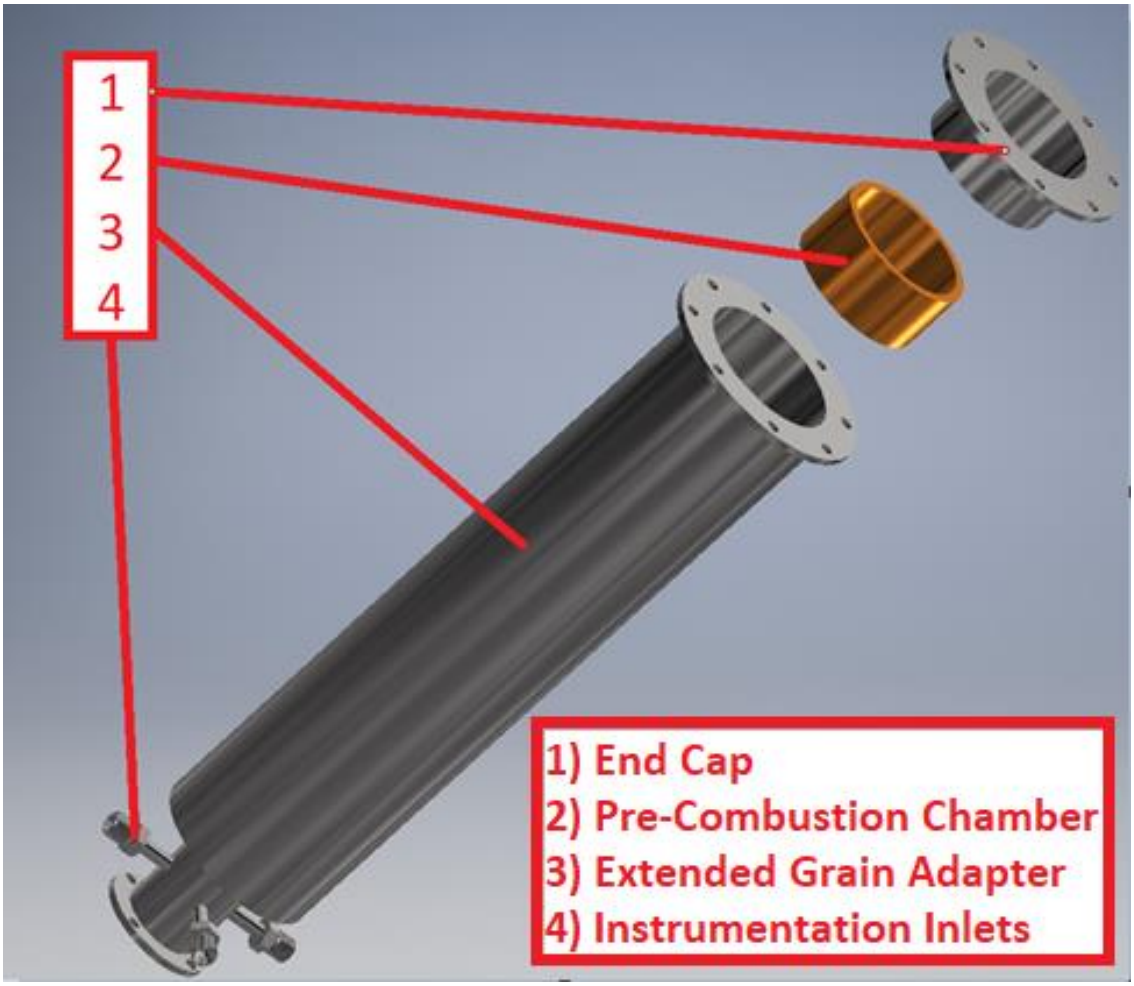

Figure 3.14: Exploded View of the High Flow Grain Adapter

The fuel grain sits between the pre-combustion chamber and the end cap, allowing the oxidizer gases to flow freely on both ends of the fuel grain, so as not to impede regression on any of the free surface of the fuel.

3.3 GOX/HTPB Test Matrix

The initial test series was designed to test four of these remaining fuel grains as a proof of concept to compare with the previous testing performed at UTEP [10]. These data also serve as a baseline for the performance of the new setup and validation of the experimental method.

Table 3.2: Proof of Concept Test Series Matrix

Test Code	Volumetric Flowrate (SLPM)	Pressure (PSI)	Burn Time (s)
HRP1-01	10±0.5	16.0 ± 5.0	10±0.1
HRP1-02	20±0.5	32.0 ± 5.0	10±0.1
HRP1-03	30±0.5	49.0 ± 5.0	10±0.1
HRP1-04	48±0.5	78.0 ± 5.0	10±0.1

Additionally, in order to prove the functionality of the system once the high flow grain adapter was installed, a quick GOX/HTPB test was performed. The results of some of these tests can be seen in Chapter 4.

3.4 HAN Decomposition Products/HTPB Test Approach

Once the viability of the system was determined with the GOX/HTPB testing, a Simulated HAN Decomposition Products/HTPB test series was designed to ascertain the baseline performance of the system. The test matrix for this system is featured in Table 3.3. This test series will incorporate not only the gases, but also steam from the steam generator.

Table 3.3: Simulated HAN Decomposition Gases/HTPB Test Matrix

Test Code	Volumetric Flowrate O2 (SLPM)	O2 Pressure (PSI)	Volumetric Flowrate N2 (SLPM)	N2 Pressure (PSI)	Burn Time (s)
HRP3-01	62±1.0	200.0 ± 5.0	64±1.0	200.0 ± 5.0	10±0.1
HRP3-02	74±1.0	200.0 ± 5.0	77±1.0	200.0 ± 5.0	10±0.1
HRP3-03	87±1.0	200.0 ± 5.0	90±1.0	200.0 ± 5.0	10±0.1
HRP3-04	99±1.0	200.0 ± 5.0	103±1.0	200.0 ± 5.0	10±0.1
HRP3-05	99±1.0	200.0 ± 5.0	103±1.0	200.0 ± 5.0	10±0.1
HRP3-06	99±1.0	200.0 ± 5.0	103±1.0	200.0 ± 5.0	10±0.1
HRP3-07	112±1.0	200.0 ± 5.0	116±1.0	200.0 ± 5.0	10±0.1
HRP3-08	124±1.0	200.0 ± 5.0	129±1.0	200.0 ± 5.0	10±0.1

3.5 Test Operations

The operation of the system is actually quite simple, first, the system is pressurized to the necessary amount for proper operations, then the lines which operate based on flow rates are set. As soon as this is done, the final step is to press the "Automatic" button on the GUI and the system performs the operations seen in Table 3.4.

Table 3.4: Hybrid Rocket Automatic Test Sequence

Time	Event	Note
0	Sparker->On, SOV-1, 2, 3, 4, 6, 101, 201, 301, 401, 601->Open	
0 to +1	Expected Ignition	
+1	SOV-3, 4, 301, 401->Closed Sparker->Off	Ignitor should be off • Abort if grain did not ignite • Abort at any time if it can be seen that the PVC casing is on fire • Appendix 5 details a more in-depth description of when to abort the test
+1.5	SOV-6, 601->Closed	
+11	SOV-1, 2->Closed SOV-10, 20->Open	*Initiates Purge Grain should be extinguished
+31	SOV-10, 20, 101, 201->Closed	Secures Purge
+32	Sequence End	

As can be seen, there are three distinct phases of igniting the grain:

1. Ignitor ignition
2. Diffusion flame ignition
3. Self-sustained hybrid combustion

These phases are also visually represented in Figure 3.15.

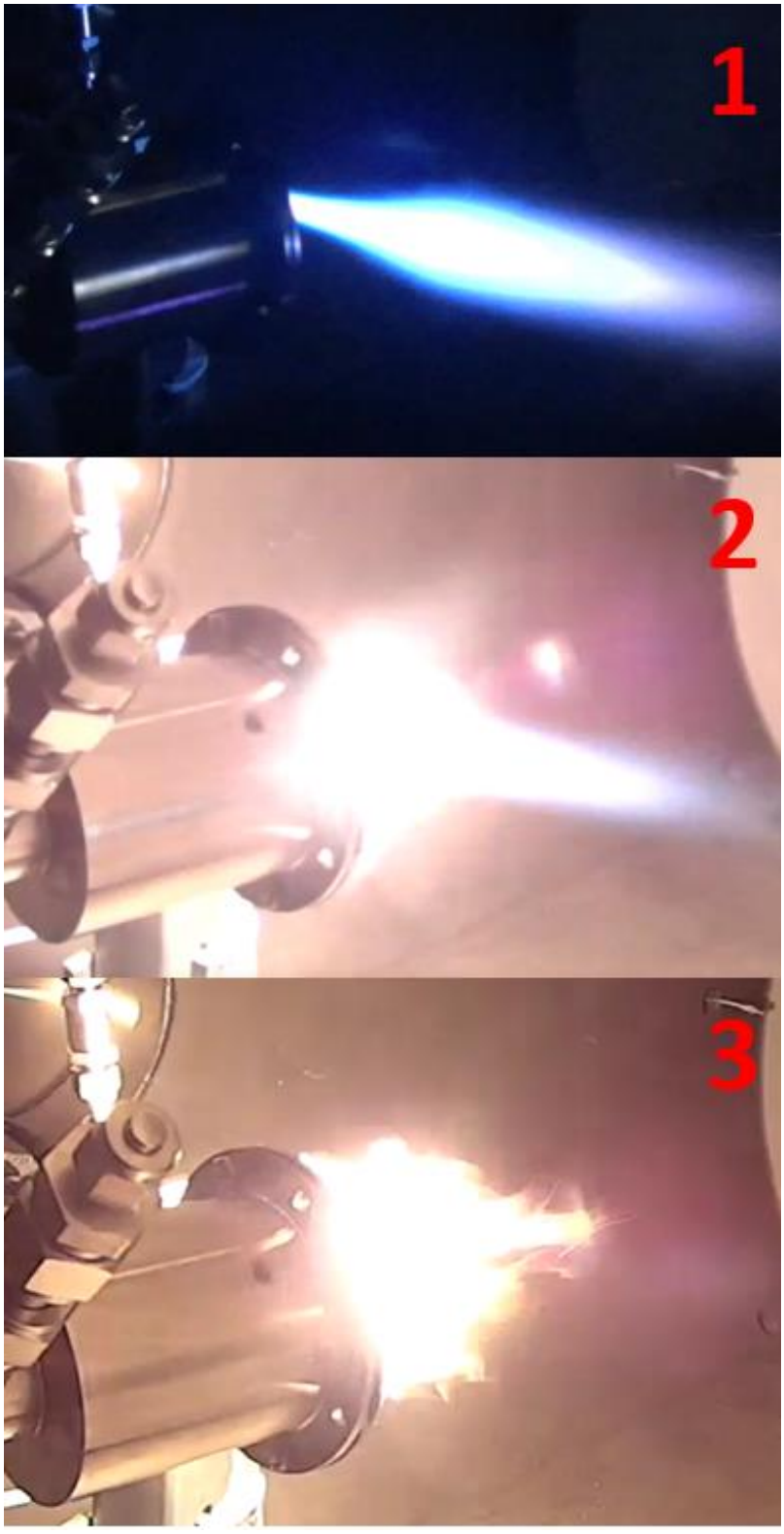

Figure 3.15: Three different phases of ignition (1) Ignitor ignition (2) Diffusion flame ignition (3) Self-sustained hybrid combustion

This is a very generalized overview of test operations, and the full test procedure can be seen in Appendix B.

Chapter 4: Results and Analysis

4.1 Alterations to Testing Scope

As these things usually go, a series of unplanned events forced the team to adjust the planned testing series. First, the manufacture of the larger scale fuel grains experienced issues. The first batch was cast using 3D printed molds, which worked well, however, the team was unable to remove the center rod, rendering the batch unusable. The second batch was cast using a steel mold, however, the fuel did not cure correctly and had a very gooey, spongy consistency. It is believed that the improper curing of these grains was caused by a mold release agent that was applied to the surface of the mold to more easily remove the fuel grains.

Due to deadlines, it was decided to move forward with testing using the low flow fuel grain adapter, since there were spare motors from previous experiments, and use it to perform the test matrix featured in Table 3.3. The system was reconfigured to make perform this testing, but the system was still unable to achieve grain ignition due to the high-volume percentage of nitrogen and steam in the oxidizer mixture. Further research and study of the CEA Analysis in Appendix A, as well as comparison of this information with studies that have thermally and catalytically decomposed HAN [19] reveals that the CEA analysis might not be accurate. Previous experience trying to use CEA for liquid propellants, such as AF-M315E, have shown that the code is not capable of determining the decomposition products of these chemicals. The most telling indicator is that testing has shown there is a substantial amount of HNO_3 released during HAN decomposition. Reviewing the CEA analysis has HNO_3 listed as a product that was analyzed, but considered insignificant (less than 5.0×10^{-6} mass fraction.) Further research is needed to ascertain a better HAN decomposition product gas cocktail to run through the system.

At this point it was decided to go ahead and perform a capability study on the system so that its limits would be known for future testing. This would be accomplished in two different test series, the first would be to run oxygen and nitrogen through the system, increasing the nitrogen content with each test, to figure out at what percentage the grain would no longer be able to ignite due to oxygen starvation. The second test series would use the results of the first test series as a starting point, adding steam to the mixture to figure out the maximum amount of steam that could be introduced before the grain would no longer ignite. The details of this testing will be presented in Section 4.3 of this document.

4.2 Proof of Concept Test Results

The proof of concept test was mainly designed as a functionality check of the system to ensure that it could flow oxidizer, light a diffusion flame, and subsequently sustain the hybrid fuel grain burning. It allowed for the team to practice testing the system, troubleshooting, and smooth out potential issues before actual testing of the system began. The testing went well, and the final two fuel grains were tested at the same parameters as the original low flow system for comparison, as seen in Table 4.1 below.

Table 4.1: Proof of Concept Test Results

Motor #	Initial Weight (g)	Final Weight (g)	DeltaM (g)	DeltaV (cm3)	Length (cm)	Initial Diameter (cm)	Final Diameter (cm)	Burn Time (s)	Regression Rate (cm/s)	Mass flow (g/s)
1	351.5	348.0	3.5	3.763	4.4	1.11	1.52	10	0.0207	1.049
2	353.5	349.7	3.8	4.086	4.4	1.11	1.55	10	0.0222	1.049

This data was compared to the data from a previous study at UTEP [10], and also compared to data from a study by Deluca, et. al., [29] and pictured in Figure 4.1.

Figure 4.1: A Comparison of the Proof of Concept Testing to Previous Testing Data and Literature [10,29]

4.3 Capability Study Test Results

As previously discussed, a capability study was run on the system to ascertain its effectiveness at combusting mixtures of oxygen, nitrogen, and steam, as those are the most common decomposition products of HAN and AF-M315E. The purpose of the first series of tests was to figure out what the highest nitrogen to oxygen ratio the system could run at before becoming oxygen starved. It was known from a previous test series that the grain would ignite in a 50/50 nitrogen/oxygen environment, so that was used as the starting point for this series, the results of which can be seen in Table 4.2.

Table 4.2: Gas Mixture Testing Results

Test #	Test Article	O2 %	O2 Flow (LPM)	N2 %	N2 Flow (LPM)	Ignition?
1	102	50	50	50	56	Y
2	103	45	45	55	62	Y
3	104	40	40	60	68	N

Test #3 was repeated several times to ensure that its non-ignition was not an anomaly. With this data in hand, the second test series used the first series as a starting point. This second series involves adding steam to the oxidizer mixture and attempting to ignite the grain to see what the maximum amount of steam each mixture ratio can handle. While advancing through the test series, a “stair-step” method was used, after it was determined that the grain would not ignite, the oxygen content was increased and the amount of steam that caused the previous mixture to fail was used as the starting point so as to minimize the number of tests and reduce runtime on the system. The results of each of these tests are reported in Table 4.3.

Table 4.3: Steam Mixture Testing Results

O45N55								
Test #	Test Article	O2 %	O2 Flow (LPM)	N2 %	N2 Flow (LPM)	Stm %	Stm Flow (LPM)	Ignition?
1	104-I	45	45	55	62	2E-05	0.005	Y
2	105-I	45	45	55	62	4E-05	0.010	N
O55N45								
Test #	Test Article	O2 %	O2 Flow (LPM)	N2 %	N2 Flow (LPM)	Stm %	Stm Flow (LPM)	Ignition?
1	106-I	55	55	45	51	4E-05	0.010	Y
2	107-I	55	55	45	51	6E-05	0.015	Y
3	108-I	55	55	45	51	8E-05	0.020	Y
4	101-II	55	55	45	51	0.0001	0.025	N
O65N35								
Test #	Test Article	O2 %	O2 Flow (LPM)	N2 %	N2 Flow (LPM)	Stm %	Stm Flow (LPM)	Ignition?
1	102-II	65	65	35	39	0.0001	0.025	Y
2	103-II	65	65	35	39	0.0001	0.030	Test Fail
3	104-II	65	65	35	39	0.0001	0.030	N
O75N25								
Test #	Test Article	O2 %	O2 Flow (LPM)	N2 %	N2 Flow (LPM)	Stm %	Stm Flow (LPM)	Ignition?
1	105-II	75	75	25	28	0.0001	0.030	Y
2	106-II	75	75	25	28	0.0001	0.035	N
O85N15								
Test #	Test Article	O2 %	O2 Flow (LPM)	N2 %	N2 Flow (LPM)	Stm %	Stm Flow (LPM)	Ignition?
1	107-II	85	85	15	17	0.0001	0.035	Y
2	108-II	85	85	15	17	0.0002	0.040	Y
3	101-III	85	85	15	17	0.0002	0.045	Y
4	102-III	85	85	15	17	0.0002	0.050	Y
5	103-III	85	85	15	17	0.0003	0.060	Y
6	104-III	85	85	15	17	0.0003	0.070	Y
7	105-III	85	85	15	17	0.0003	0.080	Y
8	106-III	85	85	15	17	0.0004	0.090	Test Fail
9	107-III	85	85	15	17	0.0004	0.090	Y

The test series used a naming convention O##N## which indicates the volume percentage of the oxidizer gas without the steam. For instance, O45N55 indicates that the inlet gases were 45% oxygen and 55% nitrogen before steam was introduced to the mixture. The tests which were listed as “Test Fail” are due to the diffusion flame not igniting, which indicates that there wasn’t a sufficient amount of methane flow to initiate combustion of the fuel

grain. The testing series ended at 85/15 oxygen/nitrogen mixture ratio since it was able to achieve combustion with 0.090 LPM steam flow, which is the maximum pumping power that the steam generating system can produce. All of this data was compiled into Figure 4.2, seen below.

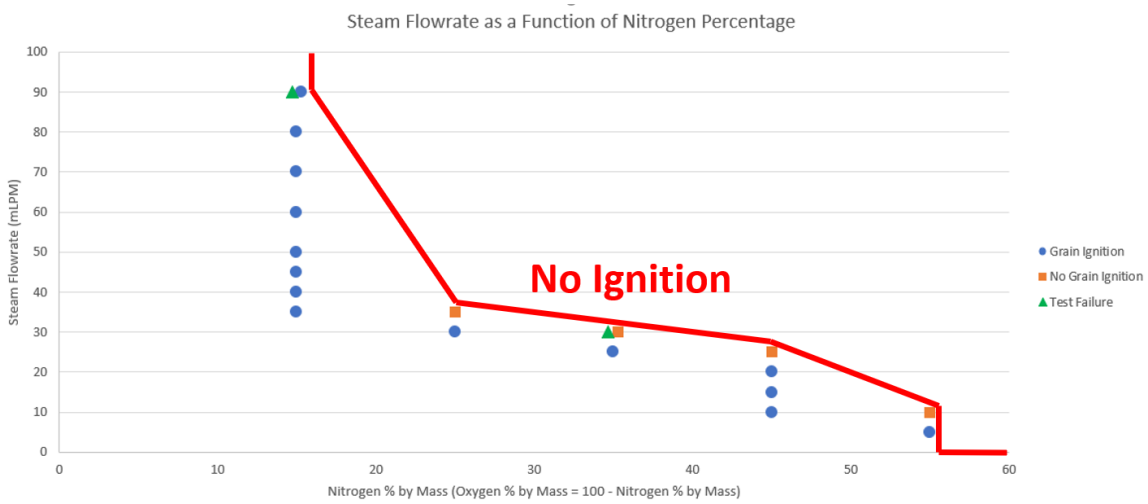

Figure 4.2: Graphical Results of Capability Testing

In this chart, the blue dots represent tests where the grain ignited and burned for the duration of the test, the orange squares are the tests where the diffusion flame lit, but there was no subsequent grain ignition, and lastly, the green triangles are considered "Test Failures" because the diffusion flame did not ignite. This data shows the maximum amount of steam flow that can be present in the system and still ignite the fuel grain. Once the amount of pure oxygen in the system reached 85%, the mixture was able to light at the highest steam flow rate possible with the pumps being used in the system, so it is assumed that all oxidizer combinations higher than this will be able to ignite with that amount of steam flow. The area above the red line is the "No Ignition" zone which indicates the area where the grain will not be able to ignite due to a lack of available oxygen.

Video was also captured for all of the capability tests so that they could be reviewed at the leisure of the team after testing was completed. Figure 4.3 is a compilation of images of each of the successful tests, in addition to O65N35 2, a test failure, once they reached a steady state combustion.

Figure 4.3: Compilation of Images During Testing

Test O65N35 2 was interesting in that the grain was able to briefly ignite, but was quickly extinguished, which resulted in it being considered a failure.

4.4 Regression Rate

Regression rate data was recorded for the Capability Test series, this data can be seen in Table 4.4.

Table 4.4: Regression Rate Data for Capability Testing

Motor #	Initial Weight (g)	Final Weight (g)	DeltaM (g)	DeltaV (cm3)	Length (cm)	Initial Diameter (cm)	Final Diameter (cm)	Burn Time (s)	Regression Rate (cm/s)
104-I	344.5	344.3	0.2	0.215	4.455	1.697	1.715	10	0.001
105-I	349.8	349.8	0.0	0.000	4.592	1.518	1.518	10	0.000
106-I	350.9	350.7	0.2	0.215	4.483	1.433	1.454	10	0.001
107-I	341.5	341.4	0.1	0.108	4.426	1.561	1.571	10	0.000
108-I	345.4	345.0	0.4	0.430	4.445	1.736	1.771	10	0.002
101-II	351.6	351.6	0.0	0.000	4.551	1.469	1.469	10	0.000
102-II	350.3	347.0	3.3	3.548	4.605	1.551	1.840	10	0.014
103-II	349.2	349.2	0.0	0.000	4.422	1.469	1.469	10	0.000
104-II	344.3	344.3	0.0	0.000	4.455	1.805	1.805	10	0.000
105-II	349.8	346.5	3.3	3.548	4.592	1.518	1.813	10	0.015
106-II	350.7	350.7	0.0	0.000	4.483	1.485	1.485	10	0.000
107-II	341.4	337.5	3.9	4.194	4.426	1.715	2.037	10	0.016
108-II	345.0	342.0	3.0	3.226	4.445	1.754	2.000	10	0.012
101-III	351.6	348.6	3.0	3.226	4.551	1.469	1.749	10	0.014
102-III	347.0	342.6	4.4	4.731	4.605	1.71	2.057	10	0.017
103-III	349.2	346.3	2.9	3.118	4.422	1.469	1.748	10	0.014
104-III	344.3	341.3	3.0	3.226	4.455	1.805	2.044	10	0.012
105-III	346.5	343.0	3.5	3.763	4.592	1.779	2.051	10	0.014
106-III	350.7	350.7	0.0	0.000	4.483	1.485	1.485	10	0.000
107-III	337.5	334.6	2.9	3.118	4.426	1.876	2.102	10	0.011

This data was plotted against the regression rate data from previous experiments at UTEP [10], and can be seen in Figure 4.4.

Figure 4.4: Regression Rate from Previous Experiments Compared to the Capability Test Series

It can be seen that the regression rate of the Capability test series falls below the projected trendline of the previous experiments. This is expected since the purpose of the Capability

test series was to push the system to its operating limits, some loss of performance is to be expected. Also, it should be noted that the regression rates of the “No Grain Ignition” and “Test Failure” tests were omitted from the chart.

The wide variations in regression rate between the different tests with little correlation between regression rate and flow rates is indicative of the lack of control over the steam input to the system. This problem and potential improvements to the system are further covered in Section 5.2.

Chapter 5: Conclusion

5.1 Summary

The scope of this project was to create a system that would scale up the efforts of UTEP's hybrid rocket propulsion project and bring the data more in line with existing literature. In summary, the results of this project are as follows:

- Designed a more robust system inside of the bunker located in UTEP's Goddard Propulsion Laboratory. This included:
    - Gas Mixing Chamber – This component takes the base gases and combines them. The barrel section of the mixing chamber was designed to be long enough so that the gases have time to homogenously mix.
    - High Flow Grain Adapter – Designed to contain the upscaled fuel grains and features improvements over the original grain adapter in its ability to measure pressure and the implementation of a pre-combustion chamber.
- Assess the performance of the system and fine tune the operating procedures of the system through an exhaustive testing campaign. The system was validated by comparing the data collected from low flow testing with test results from an earlier UTEP hybrid test series [10].
- Establish the infrastructure for future testing series, such as being able to change out injector heads and varying the inlet gases.

5.2 Future Work

While a great deal of progress was made, there is still a long way to go on the project before it reaches completion. Major milestones that still need to reach fruition include:

- The most vexing issue with testing stems from the steam generator's operating and reliability parameters. While performing the capability test series, several nuances with operating the steam generating system were noticed. There are so many variables that need to be controlled, it was almost impossible to keep the amount of steam flow consistent from test to test. The steam generator performed much better than the previous iteration if the system, but improvements can still be made to improve the consistency of the steam being added to the system. Going forth with testing, it would be beneficial to create a steam generating system that can reliably generate accurate amounts of steam. A concept for a more reliable steam generator can be seen in Figure 5.1.

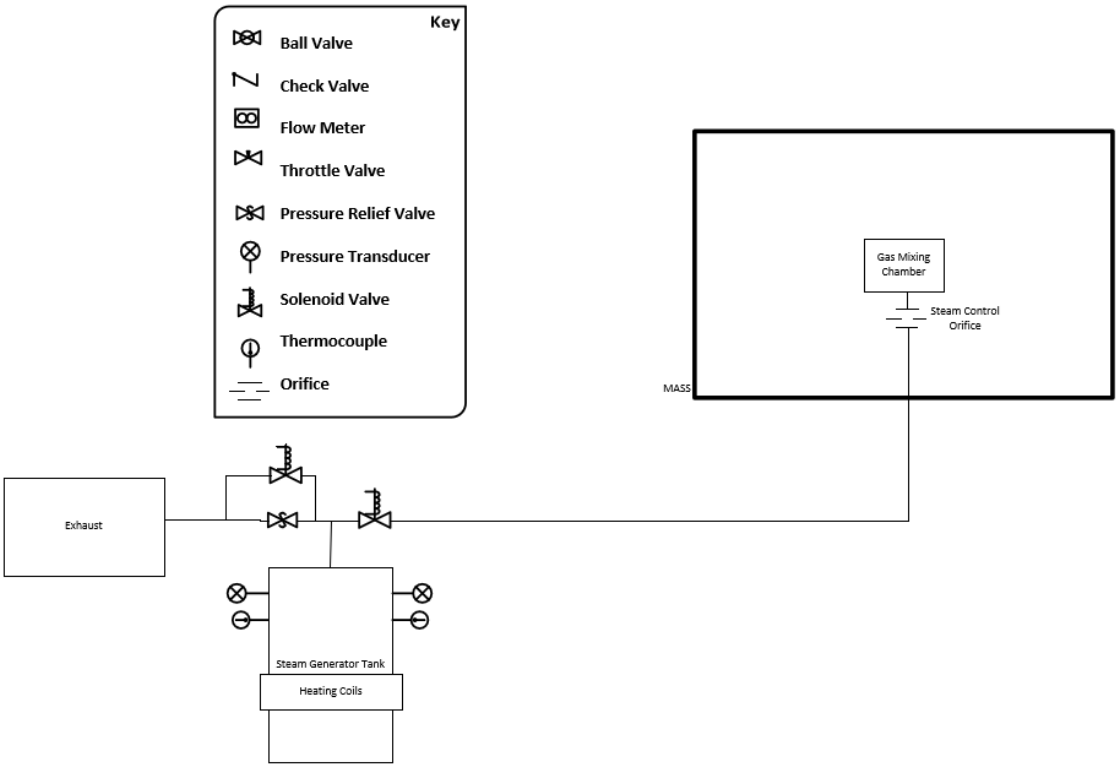

Figure 5.1: Suggested Steam Generator Upgrade

With this design, the heating coils on the steam generator tank would cycle to maintain a certain temperature in the tank. Pressure and temperature would be measured with redundant pressure transducers and thermocouples. Pressure would be controlled by a solenoid valve relieving pressure based on the pressure transducer readings, with a relief valve as the backup. When steam flow is desired, the solenoid control valve would open and send steam through the steam control orifice, which would be sized based on the steam generator tank operating pressure.

- Testing the larger scale fuel grains
- Ascertaining better metrics for the HAN decomposition gases and then implementing that gas mixture in a testing series

- Furthering the design of the new injectors, performing CFD analysis on the designs, and eventually integrating them into the system and testing their performance
- Studying the potential of varying the port diameter to increase performance of the system
- The capability testing provides a good performance measure of the system, however, it would be worthwhile to rerun each test in the series multiple times, especially after the steam generator has been upgraded, so that a regression rate study can be performed.

References

[1] Hamilton, C. J. (2011). *Views of the Solar System.* Retrieved from http://solarviews.com/eng/rocket.htm

[2] Sutton, G. P., and Biblarz, O. 2001. Rocket Propulsion Elements. 7th ed. John Wiley & Sons: New York, NY.

[3] Huzel, D. K., Huang, D. H., (1992). "Modern Engineering for Design of Liquid-Propellant Rocket Engines", *Progress in Astronautics and Aeronautics* vol. 147

[4] Brown, C. D. 1996. Spacecraft Propulsion. Washington, DC: American Institute of Aeronautics and Astronautics, Inc.

[5] Heister, H., and Wernimont, E. 2007. "Hydrogen Peroxide, Hydroxyl Ammonium Nitrate, and Other Storable Oxidizers," *Fundamentals of Hybrid Rocket Combustion and Propulsion*, Progress in Astronautics and Aeronautics, edited by M. Chiavernini and K. K. Kuo, Vol. 218, AIAA, Reston, VA.

[6] "UNITED STATES DEPARTMENT OF LABOR." Chemical Sampling Information | Hydrazine | Occupational Safety and Health Administration. https://www.osha.gov/dts/chemicalsampling/data/CH_245900.html.

[7] Mohon, L., & Dunbar, B. (2017). *Green Propellant Infusion Mission (GPIM) Overview.* Retrieved from https://www.nasa.gov/mission_pages/tdm/green/overview.html

[8] Cantwell, B. 2007. "Hybrid Rockets," Personal Collection of Cantwell, Stanford University, Stanford, California.

[9] Unknown Engineer, originated at Marshall Spaceflight Center during the 1960's, US Space and Rocket Center

[10] Patel, S.J. (2017). *Development and Verification of a Lab-Scale Green Propellant Hybrid Motor System* (Unpublished master's thesis). University of Texas at El Paso, El Paso, TX.

[11] Newlands, R. 2009. Introduction to Hybrid Design. Boston University: Boston, MS.

[12] Marxman, G. A., and Gilbert, M., "Turbulent Boundary Layer Combustion in the Hybrid Rocket," *Ninth International Symposium on Combustion*, Academic Press, New York, 1963.

[13] Marxman, G., R. Muzzy, and C. Wooldridge. "Fundamentals of hybrid boundary layer combustion." *Heterogeneous Combustion Conference*, 1963. doi:10.2514/6.1963-505.

[14] Thomas, J.C., Stahl, J. M., Morrow, G.R., Petersen, E. L. "Design of a Lab-Scale Hybrid Rocket Test Stand", 52nd AIAA/SAE/ASEE Joint Propulsion Conference, AIAA Propulsion and Energy Forum, (AIAA 2016-4965)

[15] Smoot, L. D. and Price, C. F., "Pressure Dependence of Hybrid Fuel Regression Rates," AIAA Journal, Vol. 5, No. 1, 1967. pp. 102-106.

[16] Kuo, K. K., and Chiaverini, M. 2007. "Challenges of Hybrid Rocket Propulsion in the 21st Century," *Fundamentals of Hybrid Rocket Combustion and Propulsion*, Progress in Astronautics and Aeronautics, edited by M. Chiavernini and K. K. Kuo, Vol. 218, AIAA, Reston, VA.

[17] Corthéoux, L., Amariei, D., Rossignol, S., Kappenstein, C. 2006. "Thermal and Catalytic Decomposition of HNF and HAN liquid ionic as propellants", *Applied Catalysis B: Environmental*. Volume 62. Elsevier.

[18] Corthéoux, L. et al. 2004. "Thermal and Catalytic Decomposition of HNF and HAN-based propellants", *Proceedings of the 2nd International Conference on Green Propellants for Space Propulsion*, Sardina, Italy.

[19] Chambreau, S. D., Popolan-Vaida, D. M., Vaghjiani, G. L., Leone, S. R. "Catalytic Decomposition of Hydroxylammonium Nitrate Ionic Liquid: Enhancement of NO Formation", *The Journal of Physical Chemistry Letters*, 2017 8(10), 2126-2130. doi: 10.1021/acs.jpclett.7b00672

[20] Masse, R., Spores, R. A., Kimbrel, S., Allen, M., Lorimor, E., Myers, P., McLean, C. "GPIM AF-M315E Propulsion System", 51nd AIAA/SAE/ASEE Joint Propulsion Conference, AIAA Propulsion and Energy Forum, (AIAA 2015-3753)

[21] Sanchez, L.E. (2016). *Development and Testing of Oxygen/Methane Torch Igniter Technologies for Propulsion Systems* (Unpublished doctoral dissertation). University of Texas at El Paso, El Paso, TX.

[22] Chen J. J., Chun H. C., "Investigation of Swirling Flows in Mixing Chambers," Modelling and Simulation in Engineering, vol. 2011, Article ID 259401, 15 pages, 2011. doi:10.1155/2011/259401

[23] Cengel, Y. A., Cimbala, J. M. *Fluid Mechanics: Fundamentals and applications, 3rd edition*.

[24] Altman, D., and Holzman, A. 2007. "Overview and History of Hybrid Rocket Propulsion," *Fundamentals of Hybrid Rocket Combustion and Propulsion*, Progress in Astronautics and Aeronautics, edited by M. Chiavernini and K. K. Kuo, Vol. 218, AIAA, Reston, VA.

[25] Karabeyoglu, M. A., Cantwell, B. J., Altman, D. "Development and Testing of Paraffin-Based Hybrid Rocket Fuels ", 37th AIAA/SAE/ASEE Joint Propulsion Conference and Exhibit, AIAA Propulsion and Energy Forum, (AIAA 2001-4503)

[26] Creech, M., Crandell, A., Eisenhauer, N., Marx, S., Busari, T., Link, A., . . . Pourpoint, T., "3D Printer for Paraffin Based Hybrid Rocket Fuel Grains", 53rd AIAA Aerospace Sciences Meeting, AIAA SciTech Forum, (AIAA 2015-0924)

[27] Loughborough University Additive Manufacturing Research Group. (2017). *About Additive Manufacturing.* Retrieved from http://www.lboro.ac.uk/research/amrg/about/the7categoriesofadditivemanufacturing/materialextrusion/

[28] Whitmore, S. A., Merkley D. P. "Arc-Ignition of a 70%-85% Hydrogen Peroxide/ABS Hybrid Rocket System", 53rd AIAA/SAE/ASEE Joint Propulsion Conference, AIAA Propulsion and Energy Forum, (AIAA 2017-5047)

[29] Deluca, L., Galfetti, L., Colombo, G., Maggi, F., Bandera, A., Boiocchi, M., . . . Reina, A. (2011). Time-resolved burning of solid fuels for hybrid rocket propulsion. *Progress in Propulsion Physics.*

Appendix A: HAN CEA Code

```
*************************************************************************
*******
NASA-GLENN CHEMICAL EQUILIBRIUM PROGRAM CEA2, MAY 21, 2004
BY BONNIE MCBRIDE AND SANFORD GORDON
REFS: NASA RP-1311, PART I, 1994 AND NASA RP-1311, PART II, 1996
*************************************************************************
*******
problem
hp p, psia=14.7, t,c=180
react
oxid=HAN wt=0.95
oxid=H2O(L) wt=0.05 t,c=22
output massf
end

OPTIONS: TP=F HP=T SP=F TV=F UV=F SV=F DETN=F SHOCK=F REFL=F
INCD=F
RKT=F FROZ=F EQL=F IONS=F SIUNIT=T DEBUGF=F SHKDBG=F
DETDBG=F TRNSPT=F

T,K = 453.1500

TRACE= 0.00E+00 S/R= 0.000000E+00 H/R= 0.000000E+00 U/R= 0.000000E+00

P,BAR = 1.013525

REACTANT WT.FRAC (ENERGY/R),K TEMP,K DENSITY
EXPLODED FORMULA
: HAN 0.950000 -0.530179E+04 298.15 0.0000
H 4.00000 N 2.00000 O 4.00000
: H2O(L) 0.050000 -0.344044E+05 295.15 0.0000
H 2.00000 O 1.00000

SPECIES BEING CONSIDERED IN THIS SYSTEM
(CONDENSED PHASE MAY HAVE NAME LISTED SEVERAL TIMES)
LAST thermo.inp UPDATE: 6/04/15

g 6/97 *H g10/01 HNO tpis89 HNO2
g 5/99 HNO3 g 4/02 HO2 tpis78 *H2
g 8/89 H2O g 6/99 H2O2 g 5/97 *N
g 4/99 *NH g 3/01 NH2 tpis89 NH3
tpis89 NH2OH tpis89 *NO g 4/99 NO2
j12/64 NO3 tpis78 *N2 g 5/99 N2H2
tpis89 NH2NO2 g 4/99 N2H4 g 4/99 N2O
```

g 4/99 N2O3 tpis89 N2O4 g 4/99 N2O5
tpis89 N3 g 4/99 N3H g 5/97 *O
g 4/02 *OH tpis89 *O2 g 8/01 O3
g11/99 H2O(cr) g 8/01 H2O(L) g 8/01 H2O(L)

O/F = 0.000000

EFFECTIVE FUEL EFFECTIVE OXIDANT MIXTURE
ENTHALPY h(2)/R h(1)/R h0/R
(KG-MOL)(K)/KG -0.14792914E+03 -0.14792914E+03 -0.14792914E+03
KG-FORM.WT./KG bi(2) bi(1) b0i
*H 0.45116554E-01 0.45116554E-01 0.45116554E-01
*N 0.19782855E-01 0.19782855E-01 0.19782855E-01
*O 0.42341132E-01 0.42341132E-01 0.42341132E-01
POINT ITN T H N O
1 13 2499.197 -12.630 -14.601 -15.553
THERMODYNAMIC EQUILIBRIUM COMBUSTION PROPERTIES AT
ASSIGNED
PRESSURES
CASE =
REACTANT WT FRACTION ENERGY TEMP
(SEE NOTE) KJ/KG-MOL K
HAN 0.9500000 -44081.800 298.150
H2O(L) 0.0500000 -286056.128 295.150
O/F= 0.00000 %FUEL=100.000000 R,EQ.RATIO= 0.532775 PHI,EQ.RATIO=
0.000000
THERMODYNAMIC PROPERTIES

P, BAR 1.0135
T, K 2499.20
RHO, KG/CU M 1.1325-1
H, KJ/KG -1229.96
U, KJ/KG -2124.88
G, KJ/KG -31527.3
S, KJ/(KG)(K) 12.1228
M, (1/n) 23.219
(dLV/dLP)t -1.00648
(dLV/dLT)p 1.1698
Cp, KJ/(KG)(K) 3.6861
GAMMAs 1.1448
SON VEL,M/SEC 1012.2
MASS FRACTIONS
*H 0.00009
HO2 0.00005
*H2 0.00055
H2O 0.38688

*NO 0.01599
NO2 0.00002
*N2 0.26962
*O 0.00458
*OH 0.02611
*O2 0.29612
* THERMODYNAMIC PROPERTIES FITTED TO 20000.K
PRODUCTS WHICH WERE CONSIDERED BUT WHOSE MASS FRACTIONS WERE LESS THAN 5.000000E-06 FOR ALL ASSIGNED CONDITIONS
HNO HNO2 HNO3 H2O2 *N
*NH NH2 NH3 NH2OH NO3
N2H2 NH2NO2 N2H4 N2O N2O3
N2O4 N2O5 N3 N3H O3
H2O(cr) H2O(L)
NOTE. WEIGHT FRACTION OF FUEL IN TOTAL FUELS AND OF OXIDANT IN TOTAL OXIDANTS

Appendix B: Test Procedure

Bunker Test Setup Configuration

1. Turn on power supplies (electrical components must be on for at least 30 minutes prior to testing)
2. Verify that all gas K-bottle are properly strapped to the cylinder rack
3. Place “Testing in Progress” sign on both of the outside doors of the cSETR laboratory
4. Remove all personnel that will not be part of the test from the laboratory
5. Conduct walkthrough of the laboratory to verify all electrical trip, fall, chemical, fire, or other hazards have been removed from the work area
6. Open outside bunker doors and place safety guard rails outside of laboratory, facing Hawthorne street.
7. Check that components are working correctly on the Test delivery system and leak Check tests
8. System is configured per schematic in Figure 1.
9. Ensure that the proper test sequence is loaded into the “Hybrid Test Sequence” folder on the Desktop of the Control Room computer. This file needs to be named “Test Sequence” in order for the file to properly load in the GUI. The test sequences can be found in the “Test Sequence Bank” folder also located in the Desktop of the Control Room computer. Simply copy the desired test sequence into the “Hybrid Test Sequence” folder and rename it to “Test Sequence” in order for the test sequence to run correctly.

10. Open the (Hybrid Test GUI) file on LabVIEW on the main desktop computer located in the control room.
11. Initial valve line-up check consists of having COV-1, 2, 3, 4, 6 closed.
12. Check sensors: thermocouples, pressure transducers, and flow meters must be checked for proper readings. To ensure that PT's are properly working, LabVIEW should display 14±1 psia for the PT (atmospheric pressure). To ensure that TC's are reading right the LabVIEW should display 25 ±3 Celsius (ambient temperature). To ensure flow meters are properly working, LabVIEW should display 0 LPM for the flow meters.
13. Check solenoid valves: Verify the solenoid valves are opening and closing properly using the LabVIEW interface. A clicking sound will be heard once a valve is actuated. The Test Conductor in control room will send a signal to actuate the valve. The Test Engineer in bunker hears when valve opens to verify operation. This process should be done for each of the 15 solenoid valves being used during the test (SOV-1, 2, 3, 4, 6, 10, 20, 30, 40, 60, 101, 201, 301, 401, 601.)
14. Check pressure transducer: pressure readings of the pressure transducers are reflected in LabView. It must read a pressure of 0 (ambient) psig. If a pressure transducer is disconnected, the pressure reading will be unrealistic. If LabView is reading something other than 0 psig, it is possible that there is a malfunction or the pressure transducer is not connected properly. All 5 of the PT's being used during the test will be checked for proper operation (PT-101, 201, 301, 401, 601.)
15. Check thermocouples: temperature readings of the thermocouples are reflected in LabView. It must read a temperature of 25±5 degrees Celsius, depending on

ambient temperature. If a thermocouple is disconnected the temperature reading will be unrealistic. If LabView is reading something other than 25±5 degrees Celsius it is possible that there is a malfunction or the thermocouple is not connected properly. All 5 of the TC's being used during the test will be checked for proper operation (TC-1, 2, 3, 4, 6.)

16. Check camera: the view inside the MASS must be showing on the TV located inside the control room at all times.

17. Switch exhaust fan on and verify operability.

Setting Flowrates

1. Ensure exhaust fan is operating
2. Close door to the MASS
3. Open COV-1, 2, and 6
4. Set pressure regulators for lines 1, 2, and 6 to the pressure prescribed in the Test Matrix (Table 1).
5. Open SOV-1 and SOV-101 to commence flow
6. Adjust TV-1 to set the flowrate to the prescribed value in Table 1. The throttling valves are very sensitive, so care should be taken to carefully set the flowrate.
7. Once this flow rate is achieved, Shut SOV-101 then SOV-1
8. Wait at least 20 seconds for exhaust system to fully evacuate the MASS
9. Open SOV-2 and SOV-201 to commence flow
10. Adjust TV-2 to set the flowrate to the prescribed value in Table 1. The throttling valves are very sensitive, so care should be taken to carefully set the flowrate.
11. Once this flow rate is achieved, Shut SOV-201 then SOV-2

12. Wait at least 20 seconds for exhaust system to fully evacuate the MASS
13. Open SOV-6 and SOV-601 to commence flow
14. Adjust TV-6 to set the flowrate to the prescribed value in Table 1. The throttling valves are very sensitive, so care should be taken to carefully set the flowrate.
15. Once this flow rate is achieved, Shut SOV-601 then SOV-6
16. Wait at least 20 seconds for exhaust system to fully evacuate the MASS
17. Align the system per the Initial Valve Lineup in Table 2.

Table 2: Leak Check Valve Line-up

Component Type	Component ID	Configuration
Manual Ball Valve	COV-1	Closed
Manual Ball Valve	COV-2	Closed
Manual Ball Valve	COV-3	Closed
Manual Ball Valve	COV-4	Closed
Manual Ball Valve	COV-6	Closed
Manual Ball Valve	COV-10	Closed
Manual Ball Valve	COV-11	Closed
Normally Closed (NC) Solenoid Ball Valve	SOV-1	Closed
NC Solenoid Ball Valve	SOV-2	Closed
NC Solenoid Ball Valve	SOV-3	Closed
NC Solenoid Ball Valve	SOV-4	Closed
NC Solenoid Ball Valve	SOV-6	Closed
Normally Open (NO) Solenoid Ball Valve	SOV-10	Closed
NO Solenoid Ball Valve	SOV-20	Closed
NO Solenoid Ball Valve	SOV-30	Closed
NO Solenoid Ball Valve	SOV-40	Closed
NO Solenoid Ball Valve	SOV-60	Closed
NO Solenoid Ball Valve	SOV-101	Closed
NO Solenoid Ball Valve	SOV-201	Closed
NO Solenoid Ball Valve	SOV-301	Closed
NO Solenoid Ball Valve	SOV-401	Closed
NO Solenoid Ball Valve	SOV-601	Closed
K-bottle Regulator	N2 Reg	Closed, Regulator Backed Out

1. Open N2 K-bottle and set regulator to 200 psi.
2. Open COV-10, this will pressurize the purge header

3. Open SOV-10, 20, 30, 40, 60 and leave open for the duration of the leak test.
4. Allow system to pressurize to 200 $\pm$5 Psi.
5. Apply Snoop fluid to perimeter of components in lines 1, 2, 3, 4, and 6 to visually inspect for gas leaks.
6. If there is a leak, tighten site of leak.
7. If there are no leaks:
8. Close SOV-10, 20, 30, 40, 60
9. Open SOV-101, 20, 301, 401, 601
10. Close COV-10
11. Open COV-11, this will depressurize the purge header
12. Close COV-11 when all pressure from the purge header has been released

Test Procedure

1. Ensure exhaust fan is on
2. Switch camera to on position and begin recording
3. Configure the system per Initial Valve Line-up in Table 3.

Table 3: Testing Initial Valve Lineup

Component Type	Component ID	Configuration
Manual Ball Valve	COV-1	Closed
Manual Ball Valve	COV-2	Closed
Manual Ball Valve	COV-3	Closed
Manual Ball Valve	COV-4	Closed
Manual Ball Valve	COV-6	Closed
Manual Ball Valve	COV-10	Closed
Manual Ball Valve	COV-11	Closed
Normally Closed (NC) Solenoid Ball Valve	SOV-1	Closed
NC Solenoid Ball Valve	SOV-2	Closed
NC Solenoid Ball Valve	SOV-3	Closed
NC Solenoid Ball Valve	SOV-4	Closed
NC Solenoid Ball Valve	SOV-6	Closed
Normally Open (NO) Solenoid Ball Valve	SOV-10	Closed
NO Solenoid Ball Valve	SOV-20	Closed
NO Solenoid Ball Valve	SOV-30	Closed
NO Solenoid Ball Valve	SOV-40	Closed
NO Solenoid Ball Valve	SOV-60	Closed
NO Solenoid Ball Valve	SOV-101	Closed
NO Solenoid Ball Valve	SOV-201	Closed
NO Solenoid Ball Valve	SOV-301	Closed
NO Solenoid Ball Valve	SOV-401	Closed
NO Solenoid Ball Valve	SOV-601	Closed
K-bottle Regulator	N2 Reg	Closed, Regulator Backed Out

4. Set tank regulators to the pressure dictated in Table 4

Table 4: Tank Regulator Settings

Tank Number	Tank Gas	Pressure Setpoint (psi)	Flowmeter Setpoint (SLPM)
1	Oxygen	See Test Matrix	See Test Matrix
2	Nitrogen	See Test Matrix	See Test Matrix
3	Oxygen	200.0 ± 5.0	N/A
4	Methane	120.0 ± 5.0	N/A
6	Methane	100.0 ± 5.0	20 ± 0.1
Purge	Nitrogen	50.0 ± 10.0	N/A

5. Open COV-1, 2, 3, 4, and 6
6. Open COV-10
7. Close bunker doors and exit the area
8. At this time, all personnel should assume their required positions in the control room.
9. Test Supervisor: Oversee all operations.
10. Test Conductor: Computer operations
11. Test Engineer: Operate manual valves. Monitor readings provided within signal conditioners. In charge of emergency switches.
12. Start automated-sequence in LabVIEW

Table 5: Test Sequence

Time	**Event**	**Note**
0	Sparker->On, SOV-1, 2, 3, 4, 6, 101, 201, 301, 401, 601->Open	
0 to +1	Expected Ignition	
+1	SOV-3, 4, 301, 401->Closed Sparker->Off	Ignitor should be off • Abort if grain did not ignite

		• Abort at any time if it can be seen that the PVC casing is on fire • Appendix 5 details a more in-depth description of when to abort the test
+1.5	SOV-6, 601->Closed	
+11	SOV-1, 2->Closed SOV-10, 20->Open	*Initiates Purge Grain should be extinguished
+31	SOV-10, 20, 101, 201->Closed	Secures Purge
+32	Sequence End	

13. Upon completion of the automated sequence, LabVIEW will relinquish the system back to manual control
14. Check that SOV-1, 2, 3, 4, and 6 are shut

Post-Test Procedure

1. Test Engineer enters the bunker, shuts all of the K-Bottle valves and releases the pressure on the K-Bottle regulators EXCEPT FOR THE NIGTROGEN PURGE BOTTLE.
2. Test Engineer leaves the bunker and closes the bunker doors.
3. Open SOV-1, SOV-101, and SOV-10, allow line to purge with nitrogen for 20 seconds
4. Close SOV-10
5. Open SOV-2, SOV-201, and SOV-20, allow line to purge with nitrogen for 20 seconds
6. Close SOV-20
7. Open SOV-3, SOV-301, and SOV-30, allow line to purge with nitrogen for 20 seconds
8. Close SOV-30

9. Open SOV-4, SOV-401, and SOV-40, allow line to purge with nitrogen for 20 seconds
10. Close SOV-40
11. Open SOV-6, SOV-601, and SOV-60, allow line to purge with nitrogen for 20 seconds
12. Close SOV-60
13. Test Engineer enters the bunker and closes COV-1, 3, 4, and 6
14. Shut the K-Bottle valve on the Purge Tank and release the pressure on the purge regulator
15. Open COV-11 to release the pressure from the purge header
16. When pressure is released from the purge header, shut COV-11 and COV-10
17. Deenergize the system to allow the solenoid valves to return to their default configuration

Shutdown Procedure

1. Turn off exhaust fan
2. Export test data to excel and save for post processing
3. Turn off power supply boxes
4. Close LabVIEW program
5. Make sure exhaust fan is off
6. Close back bunker doors and remove guard rails
7. Remove testing signs from laboratory doors

Appendix C: HTPB Motor Creation Procedure

Scope

The AF-M315E decomposition system is designed to decompose AF-M315E, an Air Force Developed propellant, and measure the chemical makeup and concentrations of the propellant's decomposition gases. The propellant reacts with a preheated iridium coated silicon carbide foam catalyst, contained within an alumina holder. The propellant decomposes into different gases that are then passed through a heat sink to remove some heat from the gases before they are captured in a sample cylinder. After the cylinder has cooled, the gases are then analyzed with a mass spectrometer. The results of these tests will be used to replicate the decomposition gases of AF-M315E and attempt to use them as an oxidizer for a hybrid rocket propulsion system in conjunction with HTPB as the fuel.

The HTPB fuel grain will be housed inside of a combustion chamber where the simulated AF-M315E gases will flow as oxidizer and the fuel grain will be ignited. The goal of this project is to test the combustion properties of HAN-HTPB combination and improve the efficiency and regression rate of HAN-HTPB.

Procedure Objectives

Fabricate HTPB Test Articles.

- To fabricate the test articles, HTPB will be combined with a curative to create a test article with a homogenous fuel grain.
- The following procedure is to create four 250mm grains of HTPB.

Procedure logistics

Procedure Name: HTPB Test Article Fabrication
Procedure Number: _____

Procedure Date: _____

Location:

Engineering Bldg. Room M205
University of Texas at El Paso
500 W. University Ave.
El Paso, TX 79968

Personnel Breakdown and Contact Info:

Role	Name	Phone	Email
Procedure Conductor			
Procedure Operator			
Principle Investigator	Norman Love	(915)747-8981	ndlove@utep.edu
cSETR Safety Manager	Scott Hill	(915)747-8945	cshill2@utep.edu

Materials

1. Liquid HTPB Binder (R-45M)

   WEIGHT (± 1g): 1837g

2. Isophorone Diisocyanate (IPDI)

   WEIGHT (± 1g): 165g

3. Carbon Black

   WEIGHT (± 1g): 5g

4. Aluminum Foil Roll
5. Saran Wrap
6. Laboratory Scale (± 0.01g)
7. Triple Beam Balance (± 1g)
8. Steel Stirring Spatula
9. Beakers (Glass, 4 Liter)x1
10. PVC Pipe SCH 40 (Approx. 11.0 in)x4
11. HTPB Mold Base x1
12. Stainless-Steal Rodx4
13. UNC-12-2 Jam Nut x4
14. PF Degreaser
15. Acetone
16. Cheese Cloth
17. Labels x2
18. Marker

Safety Hazards

Concern No.	Concern	Initial RAC	Residual RAC	Residual Risk	Mitigating Feature
1	Exposure of personnel to toxic fumes generated by uncured propellant	3C	3E	Low	Mixing procedure will be done in a fume hood and motors will be covered with glass panel
2	Asphyxiation due to venting of IPDI, in an enclosed room results in death or injury to personnel	2C	2E	Low	Mixing procedure will be done in a fume hood and motors will be covered with glass panel

Safety Precautions

Use approved personal protective equipment (PPE):

A. Eyes: Safety goggles shall be worn during the entirety of the mixing process.

B. Ears: No hearing protection will be necessary for mixing HTPB.

C. Hands: Latex Protective gloves shall be worn during the entirety of the mixing process.

D. Clothing: A fire resistant lab coat shall be worn for the entire procedure

All personnel shall wear approved personal protective equipment for the operation being performed as defined below:

General Operations:

Eyes	Safety goggles shall be worn at all times when inside Lab M205
Feet	Closed toe shoes shall be worn at all times when inside Lab M205
Ears	No hearing protection is required in Lab M205

If any personnel injury occurs, the following is offered as a guide:

- Isolate or remove the hazard from the area.
- Move injured personnel only if necessary to prevent further injury.
- Call for medical help.
    - Medical/Ambulance 911
    - Fire Department 911
    - UTEP PD 915-747-5611
    - Environmental Incident 911
    - Medical Center 915-747-5624
    - Safety Hotline 911
    - Dr. Choudhuri 915-747-5611

Initial Checkout and Procedure

Ensure Fume hood is functional

1. Switch the fume hood power switch to “On” if it is not already in the “On” position
2. Check that air is being pulled from the fume hood by verifying that the airflow monitor is indicating “safe”
3. If any of steps 3.1.1 – 3.1.2 do not produce the expected result, abort the procedure and investigate
4. Ensure Vacuum Chamber is functional
5. Close the vacuum chamber by placing the bell jar portion on top of the chamber base
6. Open fume hood vacuum valve
7. Verify vacuum is being pulled on the chamber by physically pulling on the bell jar portion of the chamber. If there is vacuum and a good seal, the bell jar will be held firmly to the base of the chamber by the vacuum.
8. If any of steps 3.2.1 – 3.2.3 do not produce the expected result, abort the procedure and investigate
9. Ensure Oven is functional
10. Switch the oven power switch to “On”
11. Set the oven temperature controller to 100°F
12. Verify that the oven reading attains and maintains 63 ± 5°C for 5 minutes
13. If any of steps 3.3.1 – 3.3.3 do not produce the expected result, abort the procedure and investigate

Test Procedures

Mold Fabrication

1. Carefully wrap all the rods with saran wrap to prevent HTPB from sticking. Ensure that there are no creases in the saran wrap
2. Cut a wrap square place on top of the base plate covering each circle pattern
3. Insert the stainless-steel rod wrapped in saran wrap in the HTPB mold base and secure it with the jam nut. Repeat for all four rods.
4. Ensure to only make puncture big enough for the rod to pass through the saran wrap without tearing the base saran wrap
5. Make sure that the saran wrap is free of any creases before assembling the PVC pipe
6. Carefully place the PVC pipe over the assembled rod and set it in place onto the HTPB mold base
7. This mold base/saran wrap/stainless-steel rod/PVC assembly will be referred to as the “Motor Mold” or “Mold” from this point forward
8. safety walk down prior to mixing
9. Notify all personnel around and in M205 of hazardous operations
10. Ensure M205 is cleared of non-authorized personnel
11. Secure door access and all entries to Lab M205

Ingredients Weigh Up

Do not weigh ingredients more than 24 hours prior to mixing phase

For ingredient amounts, refer to 1.4 Materials

1. Cut out a square of aluminum foil (12” x 12”)
2. Lightly create a “tray” using the aluminum foil to contain carbon black
3. Using the laboratory scale, weigh the aluminum foil tray and record it as tare weight
4. Measure out the amount of carbon black using the aluminum foil “tray” and weigh using laboratory scale
5. Using the scale, weigh each container (4L beaker) and record these as tare weights
6. Clearly label each container with labels marked “R-45M” and “IPDI” to avoid confusion during the mixing phase
7. Measure out the amount of R-45M to be mixed and cover the container with aluminum foil
8. Measure out the amount of IPDI to be mixed and cover the container with aluminum foil

9. mixing
10. Place R-45M container on the center of the vacuum chamber base
11. Lock the “Bell Jar” portion of the vacuum chamber onto the base of the chamber, enclosing the R-45M container
12. Open the vacuum valve on the fume hood to pull a vacuum on the chamber
13. Watch the container inside the vacuum chamber and note the formation of a foam layer of bubbles as the vacuum increases. (Figure 2)

14. 

Figure 2: (Left) The R-45 chemical with entrained bubbles. (Middle) The bubbles being vacuumed out of the R-45 chemical. (Right) The R-45 chemical after completing the vacuum cycles and no longer containing bubbles.

15. When this layer reaches the top of the container, break the vacuum in the chamber to "pop" the bubbles that were formed
16. Repeat steps 4.4.2 through 4.4.5 until bubbles no longer reach the top of the container. When this occurs proceed to step 4.4.7 (The vacuum procedure will need to be repeated at least 10 – 20 times)
17. Set the vacuum chamber to its highest setting and leave it until all of the visible bubbles have been removed from the R-45M liquid
18. Carefully and slowly add the curative, IPDI, to the R-45M liquid to minimize the entrainment of air into the mixture
19. Carefully unload the carbon black into the two liquids
20. Mix the two liquids and carbon black thoroughly and slowly for 15 minutes with glass stirrer to minimize air entrained in the mixture
21. Place R-45M/IPDI container on the center of the vacuum chamber base
22. Lock the "Bell Jar" portion of the vacuum chamber onto the base of the chamber, enclosing the R-45M/IPDI container
23. Initiate vacuum cycle until all of the visible bubbles have been removed from the R-45M/IPDI mixture
24. Remove the mixture from the vacuum chamber
25. Slowly pour the mixture up to the mark inside the motor mold being careful not to entrain air into the mixture
26. Lock the "Bell Jar" portion of the vacuum chamber onto the base of the chamber, enclosing the motor mold
27. Initiate vacuum cycle until all of the visible bubbles have been removed from the motor mold
28. Remove the motor assembly from the vacuum chamber

29. Leave the motor assembly in the fume hood and allow for the motor mold to cure at ambient conditions
30. Clean up the mixing area as outlined in Section 4.5 of this procedure

After 24 Hours minimum

1. Place the motor mold into the oven
2. Secure the oven and set the temperature to 63°C ± 5°C and the time to the oven's maximum setting (9999 min)
3. Check the motors in the oven every 24 hours

After 7 Days

1. Remove the mold from the oven
2. Use the glass stirrer to press on the fuel grain to ensure that it has fully cured

Curriculum Vita

Travis Belcher was born in Lafayette, LA to James and Ellen Belcher. After living in several different places, domestically and abroad, he graduated from The Woodlands High School in Houston, TX in 2005. He joined the US Navy immediately after high school, and was selected for the prestigious Naval Nuclear Power Program. Upon his completion of the program, he was stationed on the USS Theodore Roosevelt where he served for four years as a Nuclear Machinist Mate. During this time, he took distance learning courses, and was later awarded a Bachelor's of Science in Nuclear Engineering Technology from Excelsior College in 2012. Upon leaving the navy at the end of his enlistment, he was hired at Space Exploration Technologies Corp. (SpaceX) as a Mechanical Test Technician for Hypergol Systems. After working at SpaceX for a while, he enrolled at Texas Tech University in May 2013 and graduated in December 2015 with a Bachelor's of Science in Mechanical Engineering. He began studying at UTEP in January of 2016. During his time at Texas Tech and UTEP he was selected for the Propulsion Academy at NASA Marshall Spaceflight Center in 2015 and was later awarded a NASA Pathways Co-op Position, also at Marshall, working as a Thermal Engineer in their Spacecraft and Vehicles Department.

Contact Information: travisb117@gmail.com

This thesis was typed by Travis Belcher